Title

DEEP INELASTIC REACTIONS: A PROBE OF THE COLLECTIVE PROPERTIES OF NUCLEAR MATTER

Authors

Moretto, L.G.
Schmitt, R.P.

Publication Date

1981-11-01

LBL-12859
Reprint

Lawrence Berkeley Laboratory
UNIVERSITY OF CALIFORNIA

Published in Reports on Progress in Physics,
Vol. 44, pp. 533-591, 1981

DEEP INELASTIC REACTIONS: A PROBE OF THE COLLECTIVE PROPERTIES OF NUCLEAR MATTER

L.G. Moretto and R.P. Schmitt

November 1981

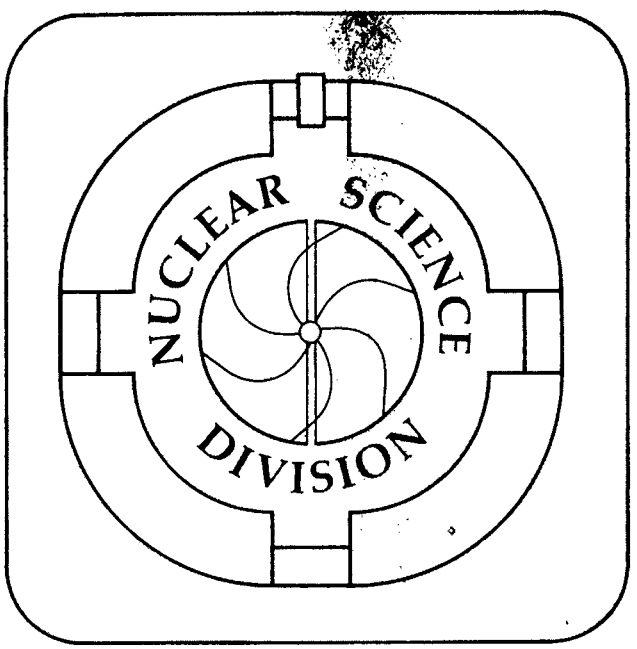

Prepared for the U.S. Department of Energy under Contract W-7405-ENG-48

DISCLAIMER

REPORTS ON PROGRESS IN PHYSICS

Deep inelastic reactions: a probe of the collective properties of nuclear matter

L G Moretto and R P Schmitt

Rep. Prog. Phys. 1981 **44** 533–91
Printed in Great Britain

The Institute of Physics

Rep. Prog. Phys., Vol. 44, 1981. Printed in Great Britain

Deep inelastic reactions: a probe of the collective properties of nuclear matter†

L G Moretto‡ and R P Schmitt§

‡ Department of Chemistry and Nuclear Science Division, Lawrence Berkeley Laboratory, University of California, Berkeley, California 94720, USA
§ Department of Chemistry and Cyclotron Institute, Texas A&M University, College Station, Texas 77843, USA

> Quibus ommibus auditis et consideratis,
> nolo verbis contendere; ad nihil enim utile est
> nisi ad subversionem audientium
> (After having listened to all sides and considered all arguments
> I do not want to argue; it would only end up confusing the listeners)
> (Augustinus *Confessions XII* 18 27)

Abstract

The general features of deep inelastic heavy-ion reactions are reviewed. The most prominent collective degrees of freedom excited in these reactions are discussed within the framework provided by the natural hierarchy of their characteristic relaxation times. Both the quantal and classical aspects of these modes are described. The limitations of the Lagrangian treatment of heavy-ion reactions are pointed out, and a more general approach using transport theory is outlined. This latter approach is illustrated by the Langevin, Master and Fokker–Planck equations. The four most widely studied collective modes are then described in detail. The damping of the relative motion is dealt with first. The general features of the energy loss spectra are described along with the energy dissipation mechanisms which have been suggested. Evidence for the thermalisation of the dissipated energy is considered. Next the discussion focuses on the mass asymmetry degree of freedom. It is shown that the complex experimental features associated with the charge distributions of the fragments can be interpreted as evidence for a diffusion process. Transport theory is applied to the charge transfer process. The coupling between the charge transfer process and the energy damping is also described and empirical prescriptions for deducing transport coefficients are discussed. Simultaneous measurements of the charge and mass of deep inelastic fragments are then considered. The roles of isospin fluctuations and giant isovector modes are analysed. Lastly, the various rotational degrees of freedom excited in heavy-ion reactions are described in connection with measurements of gamma-ray multiplicities and anisotropies and with the angular distributions of light particles and fission fragments. Both the magnitude and the alignment of the transferred angular momentum are explored.

This review was received in December 1980.

† This work was supported in part by the Nuclear Science Division of the US Department of Energy under Contract No W-7405-ENG-48.

0034–4885/81/050533+59 $06.50

Contents

1. Introduction

1.1. Why should one care about nuclear science

Historically, atomic nuclei have played a variety of roles in scientific and social thought. More frequently than not, these roles have been ancillary to some other branch of science, at least in the eyes of the non-specialists. Rutherford and Bohr used nuclei as the sturdy, though inert, pillars of their atomic models. Fermi and the scientists of the Manhattan Project introduced nuclei into a social and political role from which they have yet to recover. Mössbauer took advantage of the incredibly narrow natural width of some gamma lines to provide not only chemistry and solid-state physics, but also relativity, with a tool most exquisitely sensitive to detect minute field changes. Many other examples could be added which, under the pen of more skilled writers, would illustrate the somewhat ambiguous and perhaps tarnished image that nuclear science has in the perception of some scientists and laymen alike.

Yet, from a suitable vantage point, one quickly discovers that the nucleus stands at the crossroads of many scientific disciplines. In a single system, it incorporates features which are seen in a wide variety of other systems. This becomes apparent as soon as the quantal many-body aspects of nuclear systems are considered. Indeed, it is difficult to think of a quantal many-body system that can rival the nucleus in its richness of features. For example, superfluid ^{3}He (and ^{4}He), metals and superconductors alike find their nearly exact counterparts in the nuclear domain. So it may not be presumptuous to consider the nucleus as the many-body system 'par excellence'.

Nuclei and nuclear systems are collections of two very similar yet distinct hadrons, i.e. neutrons and protons. The density of nuclear systems in the range of excitation energy of concern to nuclear physics is such that both components can be considered strongly degenerate Fermi gases. In other words, the Pauli principle is of overwhelming importance. This feature is evident from the one-body nature of many nuclear excitations, and from the shell model of nuclear structure. The latter is a manifestation of the symmetry of the boundary conditions on the nucleonic wavefunctions dictated by the nuclear shape. The Pauli principle inhibits nucleon–nucleon scattering by blocking nearly all of the final phase space, forcing the complicated nucleon–nucleon interactions to resurface as a mean field in which nucleons move nearly independently. In this sense, the shell model is remarkably similar to the band structure of solids. In both situations the Pauli principle dominates, there is the appearance of a mean field, and shells or bands are defined by the symmetries of the nuclear shape and crystal lattice, respectively.

In the same vein, one can compare the effect of short-range interactions on pairs of fermions close to the Fermi surface in metallic superconductors and in paired nuclei. Of course, the origin of the interaction is different. While the short-range attractive electron–electron interaction in superconductors is mediated by the phonon field, the short-range attractive nuclear interaction responsible for pairing is a leftover or 'residual' part of the nucleon–nucleon interaction which is not exhausted by the mean field. Nevertheless, the overall form of the Hamiltonian is essentially the same; consequently, the physical implications are very similar. In most nuclei and superconductors the spectra of intrinsic excitations, or quasiparticles, are anomalous. In other words, there is a gap separating the ground state from the first quasiparticle excited state. The effect of the anomalous

spectrum in superconductors is well known. In nuclei, superfluid properties are particularly evident in their rotational moments of inertia at low temperature. Just as temperature breaks down superconductivity, excitation energy breaks down pairing. An analogy also exists between the collapse of superconductivity induced by a magnetic field and the collapse of pairing induced by angular momentum.

The story could go on and on, showing, as we indeed believe, that nuclear science can be identified with the rich intellectual quest to understand many-body systems. In so far as the many-body problem remains at the forefront of physical investigation so too should nuclear science.

1.2. The role of light and heavy ions in nuclear physics, old and new

The classical probes of nuclear physics are neutrons, protons, deuterons, tritons, ^{3}He and ^{4}He. Since these are very small objects compared to the average size of a nucleus, most of the nuclear reactions involving these projectiles lead to the excitation of rather elementary degrees of freedom (typically single-particle degrees of freedom) and are known as direct reactions. This mechanism is illustrated by stripping and pick-up reactions in which the projectile either adds or removes a nucleon in a well-defined quantal state in the target nucleus. The beautiful selectivity of these reactions has resulted in the development of a highly sophisticated 'particle spectroscopy'. In these reactions the shell model and its descendant, the Hartree–Fock model, has found a beautiful and challenging testing ground.

Another class of reactions occurs with light projectiles, namely compound-nucleus reactions. In these processes the projectile is absorbed by the target, producing a long-lived intermediate, or compound nucleus. During its long and undescriptive (better undescribed) life, the compound nucleus undergoes senile amnesia, forgetting all that it can about its origin without violating the conservation rules, resulting in a decoupling between the entrance channel and exit channel of the reaction. The compound nucleus decays 'statistically'; that is, the branching ratios and spectral shapes of the emitted particles are mainly determined by the available phase space for a particular decay mode. This is how statistical mechanics and thermodynamics crept into the field of nuclear physics. Since the discovery of these reactions, temperature, level density, entropy and even chemical potential have been added to the vernacular of a large number of nuclear physicists.

The dichotomy between direct reactions and compound-nucleus reactions can be seen more clearly if one considers them, respectively, as the initial and the final phase of a relaxation process. In the first case one has a simple, relatively well-defined excitation of one (perhaps a few) degree of freedom which promptly decays. In the second case, one probably begins with a simple excitation which relaxes through a hierarchy of more and more complicated nuclear excitations until it achieves equilibrium, i.e. the compound nucleus.

What is really missing in direct reactions and in compound-nucleus reactions is the story in between, namely the relaxation phase. This phase contains all the tantalising dynamical details and non-equilibrium statistical-mechanical aspects. However, even if the story in between were accessible (and it is to some extent, in the so-called pre-equilibrium decay) it would be dull if only simple nucleonic degrees of freedom were involved. However, the nucleus also exhibits some spectacular degrees of freedom which are collective, macroscopic and statistical in nature. Although these modes are not excited to any great extent by light ions, they have been known since fission made its debut to

nuclear science and to the world. To the surprised and literally flabbergasted eyes of the scientists of the time, fission showed that a nucleus could coherently evolve through a sequence of shapes, eventually leading to two fragments which are subsequently pushed apart by their mutual Coulomb repulsion. Despite the fact that fission has been intensively studied over the last 40 years, the charge and mass distributions, the sharing of the energy between translational and internal modes, the sharing of the excitation energy between the two fragments, the most obvious features of fission, have resisted the best efforts of theoreticians to understand them in a unified way.

The very slow progress in the understanding of nuclear fission is largely due to the fact that fission occurs through compound-nucleus decay. The initial conditions for all the collective motions are left to the whim of statistical fluctuations, rather than to the design of the experimenter. This fundamental inability to control the initial conditions has been the major difficulty facing the researchers in the field.

With the advent of heavy-ion reactions this difficulty has largely been removed. When two large nuclei like Kr and Au are brought into contact they do not fuse. Rather, they interact, exchanging particles, energy and angular momentum, and yet they retain their gross identities. Clearly, the same degrees of freedom involved in fission are called into play. However, now we can control many of them by adjusting the kinetic energy of relative motion, the mass asymmetry, the target and projectile neutron-to-neutron ratios, the angular momentum, and so on.

This newly found freedom has opened a new field of nuclear physics. An understanding of this new physics can occur at various levels. As expected, phenomenological models have taken the lead in interpreting the new data. But this field needs more than phenomenology. It needs to *integrate* with the conservative sectors of nuclear physics.

Therein lies the microscopic quest—the recasting of the new theories into the framework of the old well-understood spectroscopy. To be sure, we are now witnessing attempts to explain the new physics in terms of the shell model, and even in terms of nucleon–nucleon interactions as in the TDHF model (e.g. Davies *et al* 1979, Cusson *et al* 1980). The role of the giant resonances (Broglia *et al* 1974) in deep inelastic processes is prompting attempts to explain energy and angular momentum transfer with the same language used in the interpretation of the collective strength functions.

In what follows we shall review what we consider to be the most salient features of deep inelastic reactions and shall point out the relevant theoretical interpretations. Obviously, the authors of this or any other review necessarily commit some sins of omission. We hope that none of our colleagues in the field will deem our sins as mortal. To the neophyte and to the scientist in another field who desires a deeper view of the subject we suggest other reviews on the topic of heavy-ion reactions (e.g. Fleury and Alexander 1974, Galin 1976, Moretto and Schmitt 1976, Schröder and Huizenga 1977, Volkov 1978, Lefort and Ngô 1978) as well as the lists of references contained therein.

2. Collective modes excited in deep inelastic reactions and their associated relaxation times

2.1. General features of deep inelastic collisions

When two fairly massive nuclei approach each other, they must overcome both Coulomb and centrifugal barriers to make contact. If the Coulomb and centrifugal fields are sufficiently small, the two nuclei can fuse, forming a compound nucleus. However, if the dynamics is dominated by Coulomb and centrifugal effects, the nuclei, after interacting for a short time, will instead part again somewhat but not dramatically modified. We

shall restrict ourselves to collisions of this latter variety: that is, deep inelastic collisions. It is important to appreciate that the collisions considered here are 'gentle'. They involve energies of a few MeV per nucleon over the Coulomb barrier, typically < 10 MeV/A. In this regime nuclei are not shocked or shattered because the relative velocity is smaller than the various sound velocities associated with compressional or shape distortions.

To date, most of the experimental information concerning deep inelastic collisions has been obtained from the measurement of one or more of the following properties of the final reaction products: kinetic energies, charge, mass and angular distributions (for examples of early work see Kaufmann and Wolfgang 1959, Galin *et al* 1970, Artukh *et al* 1973, Moretto *et al* 1973, Kratz *et al* 1974, Hanappe *et al* 1974, Wolf *et al* 1974). Multiparameter coincidence measurements of secondary emission products (those products emitted during the de-excitation of the primary products) have also been performed providing further insight into the various properties of the short-lived di-nuclear system (or intermediate complex). From these studies, the following general features of deep inelastic collisions have emerged.

(i) The primary process is essentially binary in nature.

(ii) The final kinetic energies of the products display varying degrees of damping of the entrance channel kinetic energy, ranging from essentially elastic energies down to the Coulomb interaction energy between highly deformed fragments.

(iii) An exchange of nucleons occurs during the interaction between the two nuclei, leading to distributions in the masses of the fragments. The mass transfer process is controlled by both the interaction time and by the potential energy of the intermediate complex.

(iv) The angular distributions of projectile-like fragments are either side-peaked or forward-peaked, indicating that the interaction times are typically shorter than the rotational period of the di-nuclear system.

(v) The average neutron-to-proton (N/Z) ratio of both fragments develops towards the value which minimises the potential energy of the intermediate complex.

(vi) Angular momentum is transferred from relative orbital motion to the intrinsic spin of the two primary fragments.

(vii) The primary fragments produced in these reactions de-excite largely through the evaporation of light particles (n, p, α) and γ-rays, and occasionally via fission.

2.2. An open list of 'relevant' degrees of freedom

The experimental situation described above suggests that a wealth of new degrees of freedom is accessible to investigation. While it is tempting to list the degrees of freedom, it is difficult to define them uniquely. Some of them like the fragment separation are essential to the characterisation of the reaction and are directly connected with physical observables. Others are perhaps less essential and, in fact, may not be related to physical observables in a straightforward way. High multipole modes, associated with shape and density distributions (isoscalar) and with the distributions of neutrons and protons (isovector) in the fragments, are part of this latter class. From a theoretical standpoint these modes become less defined as their multipolarity increases in view of the surface diffuseness. A pragmatic position has often been taken in the treatment of these modes: only those modes which are directly called into cause by experimental observations should be taken into account. However, an *a priori* judgement on the relevance of a given mode has occasionally led to experiments which have substantiated the original expectations.

Consequently, without introducing any specific model, let us list some degrees of

freedom which are of demonstrated importance along with some which, in our judgement, may play an important role in the future.

(*a*) *The fragment separation distance* is well documented experimentally in terms of the asymptotic kinetic energy, even though it may not be so clearly defined for the intermediate complex.

(*b*) *The neck degree of freedom* together with the fragment separation distance is in principle of dramatic importance. Unfortunately, its relevance spreads over many observables. So far, no clear-cut experiment has characterised it.

(*c*) *The mass asymmetry* is a beautifully documented degree of freedom. The great variety of mass distributions observed experimentally has made it one of the pet degrees of freedom of this field.

(*d*) *The fragment neutron-to-proton ratios* are now the subject of intensive study. The distribution of charge at fixed mass asymmetry has a strong and direct connection with the El mode.

(*e*) *The rotational degrees of freedom* are of obvious importance in their role of determining the angular distributions. Moreover, they appear to affect the alignment of the fragment spins. While various vibrational modes (bending, twisting, wriggling and tilting) may not appear to belong to this class, they do in fact bear angular momentum and are worth considering in this category.

(*f*) *The (many) fragment deformation coordinates* may play a role in the dissipation of energy and could be responsible for part of the width of the relaxed kinetic energy peak.

(*g*) *Higher multipole isovector modes* are conceivably important in controlling the neutron-to-proton ratio of the fragments. Very little attention has been dedicated to them so far.

(*h*) *Thermodynamic degrees of freedom* such as the temperatures of the fragments may play a substantial role in view of the large degree of relaxation observed in these reactions.

2.3. Gross relaxation times

In order to follow the time evolution of the collective degrees of freedom excited in heavy reactions one needs a clock. Nature has provided one which, although not very accurate, can span incredibly short times. This clock is the angular deflection of the fragments (Nörenberg 1974, Bondorf *et al* 1974, Moretto and Sventek 1975). In reactions involving relatively light projectiles, deep inelastic reactions are confined to a fairly narrow range of impact parameters, which is limited on the lower end by the compound-nucleus formation and on the upper end by the finite radii of target and projectile. In this case, one can estimate the average angular velocity from the average angular momentum and the moment of inertia of the intermediate complex. Since the angular deflection is proportional to the time, one can then establish an approximate time scale.

This becomes more evident if one plots contours of constant cross section in the kinetic energy–angle plane (see figure 1). This plot, called a Wilczynski (1973) plot, shows a quasi-elastic ridge which moves from elastic energies at the grazing angle towards lower kinetic energies at smaller angles. Note that this ridge appears to cross 0° towards negative angles, producing the low-energy 'relaxed' ridge.

2.3.1. Kinetic energy. In order to estimate the relaxation time for the kinetic energy, let us assume that the system rotates with an angular frequency given by

$$\omega = l_{\mathrm{av}}\hbar/\mu r_0^2. \tag{2.1}$$

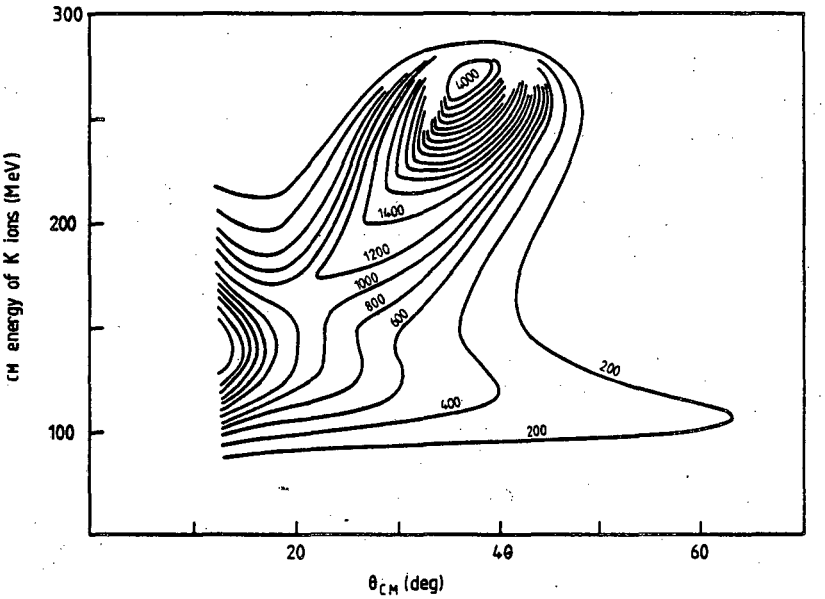

Figure 1. Contours of constant cross section in the θ_{CM}–E_{CM} plane for potassium ions (K) in the reaction $^{40}Ar + ^{232}Th$.

In this equation l_{av} is the average l value leading to a deep inelastic collision, μ is the reduced mass, and r_0 is the interaction radius. By assuming an exponential decay of the centroid of the 'quasi-elastic' component with time, one can derive the following expression for the relaxation time τ_E:

$$\tau_E = \frac{\theta_{gr} - \theta}{\omega} \left[\ln \left(\frac{\langle E(\theta_{gr}) \rangle - E_0}{\langle E(\theta) \rangle - E_0} \right) \right]^{-1} \tag{2.2}$$

where θ is the observed angle, θ_{gr} is the grazing angle, $\langle E(\theta) \rangle$ is the centroid of the ridge of cross section at angle θ, and E_0 is the centroid of the 'relaxed' component. Analysis of the data displayed in figure 1 yields $\tau_E \simeq 3 \times 10^{-22}$ s.

2.3.2. Neutron-to-proton ratio. Since most reactions involve projectiles and targets with different neutron-to-proton (N/Z) ratios, some of the earliest work in the heavy-ion field was concerned with the relaxation of these ratios (Gatty *et al* 1975, Jacmart *et al* 1975, Galin *et al* 1976). One of the first experiments involved the bombardment of ^{58}Ni and ^{64}Ni targets with ^{40}Ar and ^{40}Ca projectiles. A typical isotope yield distribution for chlorine is displayed in figure 2 for $^{40}Ar + ^{58}Ni$ reaction at an angle near the grazing. The separation between 'relaxed' and 'quasi-elastic' energy components is well-defined. In grazing (quasi-elastic) collisions, the most probable isotope formed is ^{39}Cl, which results from the stripping of a single proton from the projectile. Further examination shows that lighter isotopes tend to have lower average kinetic energies, indicating that lighter isotopes are produced in collisions involving larger energy losses and longer interaction times. In fact, the heaviest isotopes are actually missing from the relaxed component. Since the highest masses correspond to the entrance channel asymmetry N/Z, that of a neutron-rich projectile and a neutron-poor target, this indicates that the N/Z ratio has more time to relax. For angles forward of the grazing angle (see figure 2(*b*)), the two-peaked structure of the kinetic energy spectra disappears. However, the broad distributions still reflect the N/Z ratio of the relaxed component observed at the grazing angle.

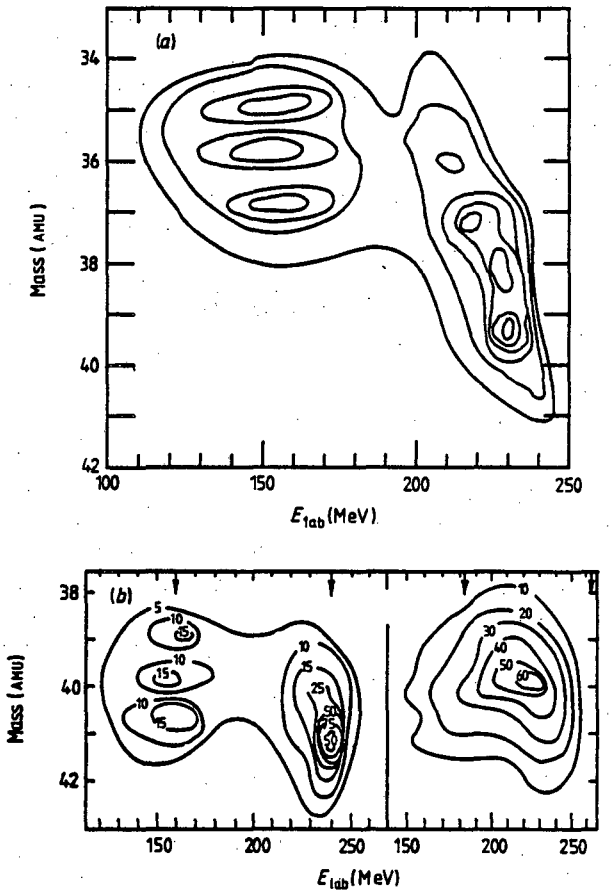

Figure 2. (*a*) Contours of constant number of events in the E_{lab}–mass plane for Cl isotopes formed in the reaction 280 MeV $^{40}Ar+^{58}Ni$. (*b*) Same as (*a*) for K isotopes at two different laboratory angles. Left: $\theta_{lab}=18°$; right: $\theta_{lab}=8°$.

After correcting for the effects of particle emission from the primary fragments, an estimate of the relaxation time, $\tau_{N/Z}$, can be made from the angular correlation observed in figures 2(*a*) and (*b*) using equation (2.2). By substituting the appropriate Z value for E, one arrives at $\tau_{N/Z} \simeq 1.3 \times 10^{-22}$ s. Comparing this with the estimate of τ_E from the preceding subsection, one immediately sees that the N/Z mode relaxes even faster than the kinetic energy.

2.3.3. Orbital angular momentum. During the course of a deep inelastic collision, angular momentum is transferred from the orbital motion of the nuclei into intrinsic spin. One way this aspect can be studied is by measuring the multiplicity of γ-rays, M_γ, emitted from the primary fragments (Albrecht *et al* 1975, Ishihara *et al* 1976, Glässel *et al* 1977, Natowitz *et al* 1978). The connection between M_γ and the spin is well known from compound-nuclear studies.

After a collision, the two primary fragments possess both excitation energy and spin angular momentum. Whilst the most efficient method for disposing of both quantities is through charged-particle emission, this de-excitation mode is strongly inhibited by Coulomb effects. Therefore, the fragments usually rely upon low l-wave neutron emission to remove the bulk of the excitation energy. After neutron emission each fragment has

approximately 8 MeV of excitation energy and most of the spin generated during the collision. A few γ-rays of El multipolarity are then emitted bringing the fragment near the lowest energy state consistent with its spin (the yrast level). For the large class of nuclei the yrast levels form collective rotational bands which decay primarily by E2 gamma emission to the next lowest level in the band. These collective (or 'stretched') E2 are emitted until the fragment reaches its ground state, removing the bulk of the spin angular momentum in the process. Thus the relationship between M_γ and the fragment spin I_1+I_2 is approximately

$$M_\gamma \cong \tfrac{1}{2}(I_1+I_2)+2a \tag{2.3}$$

where a is the number of statistical transitions per fragment.

In a macroscopic sense, one can develop a simple picture of the angular momentum transfer process. Initially the two nuclei slide upon one another. Tangential friction exerts a torque on the fragments, causing them to rotate. When the peripheral velocities are equal, the tangential friction no longer acts, and the system reaches the 'rolling' stage. Rolling friction reduces the difference in rotational frequencies of the two nuclei, resulting in rigid rotation of the complex. While both tangential and rolling friction actually act in concert, the relaxation time for the tangential friction appears to be shorter so the above description is essentially correct.

For the rolling case, the spin angular momentum of the fragments is $\frac{2}{7}$ of the total angular momentum, independent of the mass asymmetry. For rigid rotation, the fraction of the total angular momentum converted into fragment spin varies from $\frac{2}{7}$ to 1, the former for symmetric fragmentation and the latter for compound-nucleus formation. Thus rigid rotation corresponds to the equilibrium limit for the angular momentum transfer.

From inspection of figure 3 (Glässel *et al* 1977), one sees that the 90° data exhibit the pattern expected for rigid rotation. From these data, an upper limit on the relaxation time for the angular momentum transfer can be calculated. Assuming that the relaxed

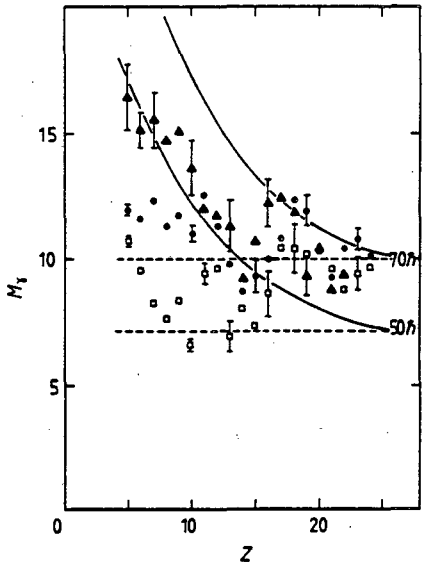

Figure 3. γ-ray multiplicities for various Z at various laboratory angles (▲, 90°; ●, 35°; □, 25°) for the reaction 175 MeV ^{20}Ne+^{107}Ag. The full curves are the values expected for rigid rotation for two l values. The broken lines correspond to the rolling limit.

energy component for the entrance channel asymmetry observed at $\theta_{lab}=90°$ corresponds to systems which have orbited through 0°, the total angle through which the complex has rotated is 150°. For this asymmetry the rotational frequency for rigidly rotating touching spheres is 10×10^{22} deg s^{-1} for $l=70\hbar$. Therefore, one obtains an upper limit on the relaxation time of

$$\tau_l=\Delta\theta/\omega=15\times10^{-22}\text{ s}.$$

2.3.4. Charge (mass) distributions. The charge or mass distributions for deep inelastic reactions display the following characteristics.

(i) At angles near the grazing the measured charge distributions are narrow, indicating very short iteration times. The centroids of the distributions coincide with the projectile Z.

(ii) At forward angles, the distributions are somewhat broader. Drift of the centroid may or may not be observed.

(iii) At backward angles, the distributions are very broad, and measurable drifts of the centroid are often seen.

If the charge distribution were relaxed, one would observe distributions similar to those seen in fission, i.e. the yield for a given Z would depend upon the potential energy of the saddle point shape through which the system must evolve in order to produce the specified asymmetry Z. An example of this ridge line potential is shown in figure 4 (Russo *et al* 1977). The probability of decaying with asymmetry Z depends upon the potential, $V(Z)$, through the density of states at the saddle point, ρ, which is a function of the excitation energy and of the shape:

$$Y(Z)\propto\rho(E-V(Z)) \tag{2.4}$$

where E is the excitation energy of the corresponding compound nucleus. If $V(Z)\ll E$,

$$Y(Z)\propto\exp(-V(Z)/T) \tag{2.5}$$

where T is the nuclear temperature.

A comparison of figures 4(*a*) and (*b*) indicates that the charge distributions at all observed angles are still far from equilibrium. A comparison of the data taken at 10° and 35.4° from figure 4(*b*), using appropriate substitutions in equation (2.5), results in the estimate

$$\tau_Z\cong60\times10^{-22}\text{ s}$$

which is the largest relaxation time observed thus far.

The aforementioned hierarchy in relaxation times is now complete:

$$\tau_{N/Z}\cong1.3<\tau_E\cong3<\tau_l=15<\tau_Z\cong60$$

where all times are in units of 10^{-22} s. From this hierarchy, one observes that all modes equilibrate much faster than the charge (mass) asymmetry mode. We shall see that this fact supports diffusion models which assume that the evolution of charge-asymmetry mode is a stochastic process.

3. The time dependence as an essential aspect of heavy-ion reactions

3.1. Characterisation of the dynamical regimes

Let us now consider which kind of dynamical regime should prevail in heavy-ion collisions. One of the first questions is whether a *quantum* or a *classical regime* applies. As

a statement of principle, nuclear systems are quantum mechanical since they are highly degenerate Fermi fluids. However, this does not mean that semiclassical or altogether classical approaches may not be applicable for specific collective modes. For instance, the rotational modes can be treated classically if $I \gg \hbar$. Yet, the moments of inertia will almost surely be controlled by quantal features.

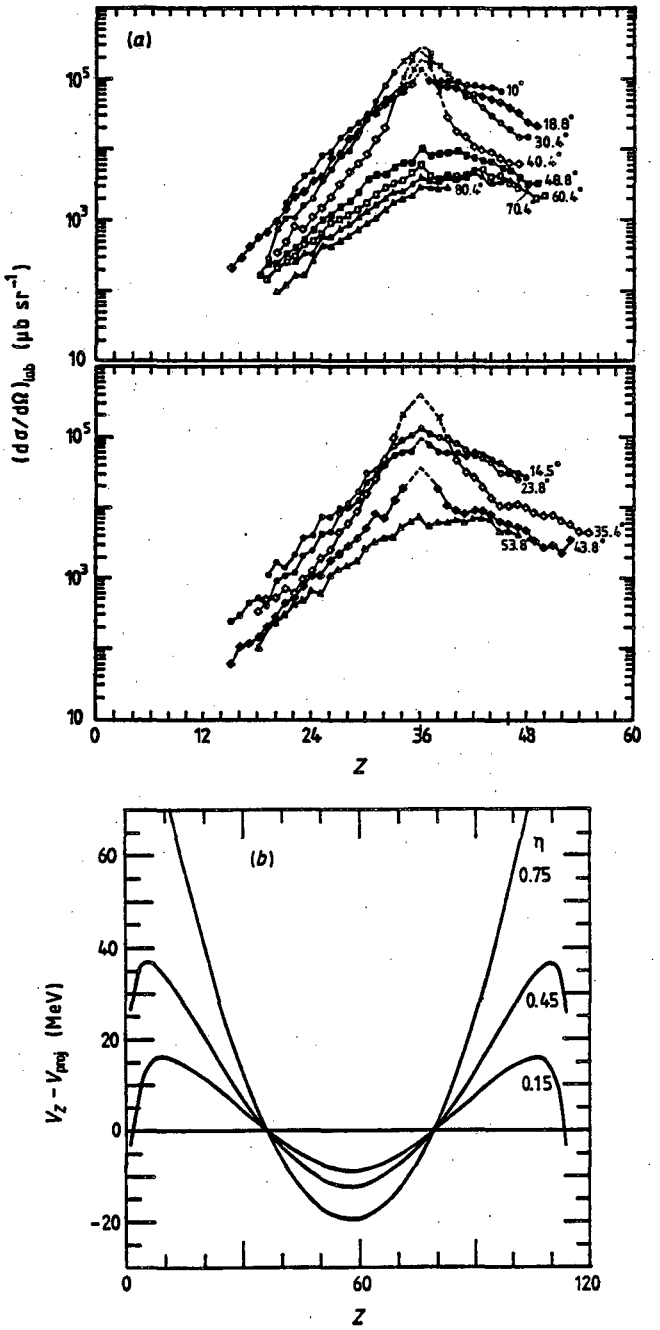

Figure 4. (*a*) Laboratory cross section as a function of Z for the reaction ^{197}Au+620 MeV ^{86}Kr at various laboratory angles. ×, uncertain decomposition from quasi-elastic. (*b*) Liquid drop potential energy of two touching spheres for ^{197}Au+^{86}Kr for various angular momenta ($\eta = l/l_{max}$).

The treatment of low multipole vibrations depends upon the sharpness of their strength function. The presence of sharp peaks dictates, at least at low temperature, a quantal treatment (Broglia *et al* 1974, 1976). On the other hand, if the strength function becomes very broad, the coordinate cannot be properly quantised, because one loses the ability to define its kinetic energy or its inertia (classically the mode is over-damped). In this case the coordinate is no longer a dynamical variable and can be treated as a parameter characterised by the potential energy alone. Thus, the associated distribution should be a classical Boltzmann distribution (Moretto *et al* 1979).

3.2. Lagrangian and diffusive approaches to the description of time-dependent processes

The fission process has been one of the first nuclear processes to be treated in a time-dependent fashion. Many authors have described the time evolution from saddle to scission point by introducing a Lagrangian in the collective variables, using the liquid drop model for the potential energy, and assuming irrotational flow to calculate the inertia tensor (e.g. Nix and Swiatecki 1965, Nix 1969). In principle, these calculations can be extended to heavy-ion reactions. In fact, this has been done (e.g. Nix and Sierk 1977). It is not clear, however, if this approach is sufficiently general.

The Lagrangian approach establishes a point-to-point correspondence between the initial and the final phase space and thus is completely deterministic. The trajectory, in a Lagrangian formulation, is a well-defined entity: for a given initial condition (point in phase space) there is one and only one trajectory.

While such an approach, generalised by including the Rayleigh dissipation function to handle viscous forces, is applicable in some cases, it actually has serious deficiencies which prevent it from describing the overall evolution of the shape parameters in heavy-ion reactions. The shortcomings of the Lagrangian approach arise from the neglect of the internal degrees of freedom. If one considers an ensemble of systems, all having the same initial conditions in collective phase space, their time evolution will be described by not one but a set of diverging trajectories because of the unspecified initial conditions of the internal degrees of freedom. Therefore, an accurate description of the time evolution of the ensemble cannot be completely deterministic, but must also contain the statistical influence of the internal degrees of freedom in determining the distribution of the elements of the ensemble in collective phase space.

One can look at this problem more concretely as follows. After the kinetic energy is dissipated, the intermediate complex has a temperature that may range, typically, between 1 and 4 MeV. As this system follows a Lagrangian trajectory in collective phase space with a few tens of MeV kinetic energy, it is subjected to random Brownian impulses which are comparable to the momentum of the system along the collective coordinate. Consequently, the Lagrangian trajectory is seriously perturbed, causing the actual trajectories of the various elements of the ensemble to diverge.

The key problem is then associated with the handling of fluctuations arising from the action of the degrees of freedom which are not explicitly taken into account. This subject belongs to the vast and still developing field of non-equilibrium statistical mechanics. We shall illustrate two equations which have been used in dealing with heavy-ion dynamics, namely the Langevin equation and the Master equation, together with its offspring the Fokker–Planck equation.

3.3. Langevin analysis

Let us consider the simplest case of a collective mode in the absence of a conservative

force (the generalisation is left to the diligent reader). The equation of motion can be written as

$$M\,\mathrm{d}v/\mathrm{d}t = F(t)$$

where v is the velocity, M is the inertia and $F(t)$ is the force. This force can be written as

$$F(t) = -kv + f(t). \tag{3.1}$$

The first term is the long time average (frictional force) and the second is the fast fluctuating component (Brownian force).

We can rewrite the above equation as

$$\frac{\mathrm{d}v}{\mathrm{d}t} + \frac{v}{\tau} = A(t)$$

where τ is the relaxation time

Integration leads to

$$v(t) = v_0 \exp(-t/\tau) + \exp(-t/\tau) \int_0^t \exp(y/\tau)\, A(y)\, \mathrm{d}y. \tag{3.2}$$

In order to proceed we need to make the following assumptions:

$$\overline{A(t)} = 0;\ \overline{A(t)^2} \text{ is positive definite; and } \overline{A(t_1)\,A(t_2)} = 0$$

except when $t_2 \cong t_1$. The bars indicate time averages. The first assumption stems from the decomposition in equation (3.1). The second implies that the system has short memory as compared to τ. The third says that the fluctuating component of the force is sizeable.

Taking the time average of equation (3.2) we obtain

$$\overline{v(t)} = v_0 \exp(-t/\tau) + \exp(-t/\tau) \int_0^t \exp(y/\tau)\, \overline{A(y)}\, \mathrm{d}y = v_0 \exp(-t/\tau).$$

We see that the mean velocity tends to zero for large times. On the other hand, if we consider the mean square velocity we obtain

$$\overline{v^2(t)} = v_0^2 \exp(-2t/\tau) + C[1 - \exp(-2t/\tau)] = v_0^2 \exp(-2t/\tau) + (T/M)\,[1 - \exp(-2t/\tau)]$$

where we have set $C = T/M$ in order to make the long time behaviour coincide with the equilibrium limit. The temperature T is associated with the thermostat composed of the microscopic degrees of freedom. This result is interesting because it coincides with the Lagrangian limit for $t \ll \tau$ and tends towards statistical equilibrium for $t \gg \tau$.

Additional integration of equation (3.2) and taking the mean square average for the coordinate gives

$$\overline{x^2(t)} = v_0^2\tau^2[1 - 2\exp(-t/\tau) + \exp(-2t/\tau)]$$
$$+ (T\tau^2/M)\,[-3 + 4\exp(-t/\tau) - \exp(-2t/\tau)] + (2\tau T/M)\,t$$

Again notice that for $\tau \gg t$

$$\overline{x^2(t)} \cong v_0^2 t^2$$

and inertia dominates the picture. On the other hand, for $t \gg \tau$

$$\overline{x^2(t)} \simeq (2\tau/M)\,Tt.$$

This is the well-known random walk result, which dominates the picture in the long time limit. In this framework one can attempt to describe both energy damping and the time evolution of a large class of collective degrees of freedom associated with deep inelastic reactions.

3.4. Master equation and Fokker–Planck analysis

Although these nearly equivalent equations have been applied to a number of degrees of freedom, they have been most extensively applied in the analysis of the mass distributions (Nörenberg 1974, 1975, 1976, Moretto and Sventek 1975). Therefore, we are going to present them in a form directly applicable to the mass asymmetry coordinate x. In its simple form the Master equation describes the time evolution of a population $\varphi(x, t)$ as follows:

$$\dot{\varphi}(x, t)=\int \mathrm{d}x'[\Lambda(x, x')\,\varphi(x', t)-\Lambda(x', x)\,\varphi(x, t)] \tag{3.3}$$

where $\dot{\varphi}$ is the time derivative of φ and $\Lambda(x, x')$, $\Lambda(x', x)$ are the direct and inverse transition probabilities. Gain and loss terms are identifiable on the right-hand side of the equation. In words, the net increase of the population per unit time at x is the difference between the flow into x from any x' and the flow outward from x into any x'. To proceed one must make assumptions about the Λ. If the Λ are space local and time-independent they will obey additional statistical assumptions, like

$$\Lambda(x, x')=\lambda(x, x')\,\rho_x \qquad \Lambda(x', x)=\lambda(x', x)\,\rho_{x'} \qquad \lambda(x', x)=\lambda(x, x')$$

where ρ_x, $\rho_{x'}$ are the state densities at x, x'. The Fokker–Planck approximation arises when one sets $x'=x+h$ and expands all the quantities in powers of h about x:

$$\dot{\varphi}(x, t)=-\frac{\partial}{\partial x}(\mu_1\,\varphi)+\frac{1}{2}\frac{\partial^2}{\partial x^2}(\mu_2\,\varphi). \tag{3.4}$$

The quantities μ_1 and μ_2 are the first and second moment of the transition probabilities Λ, i.e.

$$\mu_1=\int h\Lambda(x, h)\,\mathrm{d}h \qquad \mu_2=\int h^2\Lambda(x, h)\,\mathrm{d}h.$$

The Fokker–Planck equation has simple analytical solutions when μ_1, μ_2 are constants and for the initial condition $\varphi(x, 0)=\delta(x-x_0)$:

$$\varphi(x, t)=(2\pi\mu_2 t)^{-1/2}\exp\{-[x-(x_0+\mu_1 t)]^2/2\mu_2 t\}. \tag{3.5}$$

Notice that the centroid of the Gaussian moves with a velocity μ_1 which can be related to the driving force $F=-V_x'$ and to the friction coefficient K by the relation $K=\mu_1 F$. The second moments $\sigma^2=\mu_2 t$ is again the well-known random walk result.

When the force is harmonic,

$$V_x=c/2(x-x_{\mathrm{sym}})^2=\tfrac{1}{2}\,ch^2$$

an analytic solution is also available:

$$\varphi(h, t)=c^{1/2}\left[2\pi T\left(1-\exp-\frac{2ct}{K}\right)^{-1/2}\exp\left(-\frac{c[h-h_0\exp(-ct/K)]^2}{2T[1-\exp(-2ct/K)]}\right)\right] \tag{3.6}$$

where we have made use of the Einstein relation $\mu_1/\mu_2=-V_x'/2T$. Notice that the solution is a Gaussian whose centroid moves following the familiar differential equation

$$\ddot{h}+\frac{K}{M}\dot{h}+\frac{c}{M}h=0$$

which, in the limit $K/M\cong c/M\gg 1$, has the solution

$$h=h_0\exp[-(c/K)\,t].$$

This corresponds to over-critical damping of the motion. Similarly the second moment is given by

$$\sigma^2=\frac{T}{c}\left[1-\exp\left(-\frac{2ct}{K}\right)\right].$$

In the limit $t<\tau=K/c$

$$\sigma^2\cong 2Tt/K$$

the spreading is similar to that of a random walk. On the other hand, for $t\gg K/2c$

$$\sigma^2=T/c$$

which is the statistical equilibrium limit.

The difficulties arise in the choice of the transition probabilities. Assuming that no doorway states play any special role, the golden rule implies that

$$\Lambda(x, x')=\lambda(x, x')\,\rho_x$$

where $\lambda(x, x')$ is the microscopic transition probability and ρ_x is the level density of the configuration associated with x. On general grounds one could guess the form

$$\Lambda(x, x')=\kappa f\frac{\rho_x}{(\rho_x\rho_{x'})^{1/2}} \qquad \text{or} \qquad \Lambda(x, x')=2\kappa f\frac{\rho_x}{\rho_x+\rho_{x'}}$$

where κf is the rate-controlling factor, related to the particle transfer rate. The transition probabilities can be written as

$$\Lambda(x, h)=\kappa f\exp(-V_x'h/2T)$$

in the former case, and

$$\Lambda(x, h)=2\kappa f\frac{\exp(-V_x'h/2T)}{\exp(-V_x'h/2T)+\exp(V_x'h/2T)}$$

in the latter case.

Assuming that only adjacent configurations are coupled by the transfer of uncorrelated particles, one obtains

$$\mu_1=-2\kappa f\sinh V_x'/2T\cong-\kappa f\,V_x'/T$$

$$\mu_2=2\kappa f\cosh V_x'/2T\cong 2\kappa f$$

in the former case, and

$$\mu_1=-2\kappa f\tanh V_x'/2T\cong-\kappa f\,V_x'/T$$

$$\mu_2=2\kappa f$$

in the latter case. In both cases the Einstein relation is approximately satisfied (i.e. $\mu_1/\mu_2=V_x'/2T$).

Alternatively, if particle transfer is specifically assumed to be to the doorway state, one can consider the transfer of a particle between two fragments with chemical potential differing by an energy $a=V'h$. The transition probability is then (Moretto 1978)

$$\Lambda(x, h)=\kappa f\int\frac{d\varepsilon}{1+\exp(\varepsilon-a)/T}\left(1-\frac{1}{1+\exp(\varepsilon/T)}\right)=\kappa f\frac{V_x'h}{1-\exp(-V_x'h/T)}.$$

From this we obtain

$$\mu_1=-\kappa f\,V_x' \qquad \mu_2=\kappa f\,V_x'\coth V_Z'/2T\cong 2\kappa fT.$$

Again the Einstein relation is approximately satisfied.

The foundation and applicability of transport equations to heavy-ion collisions have been the subject of a large amount of theoretical work that cannot be reported here. The inquisitive reader will find a more profound analysis and documentation of this problem in Nörenberg and Weidenmuller (1980).

4. The damping of the relative motion

4.1. General features of the energy spectra

Terms like deep inelastic scattering and strongly damped collisions tend to emphasise the very large energy losses which can occur in heavy-ion reactions. As advertised earlier the centroids of the fully relaxed peaks are close to the Coulomb repulsion energy for touching fragments. This can be seen in figure 5 where the mean energy is plotted as a function of the atomic number of the projectile-like fragment (Moretto *et al* 1976). The experimental data lie between the calculated curves for touching spheres and spheroids at their equilibrium deformation, indicating substantial deformations of the fragments. This trend and the observation that the mean centre-of-mass energies of the completely relaxed component is angle-independent provided the earliest evidence that the reaction is essentially binary even for large energy losses (Moretto *et al* 1973).

An examination of the energy spectra (see figure 6(*a*)) or Wilczynski diagram (figure 1) reveals a continuous range of energy losses, extending from zero to very large values. While the detailed behaviour of the energy spectra depends on the particular reaction, a number of rather general observations can be made. First of all, the energy spectra tend to be broadest for fragments with charges close to that of the projectile and at angles close to the grazing angle. For this range of masses and angles one can frequently

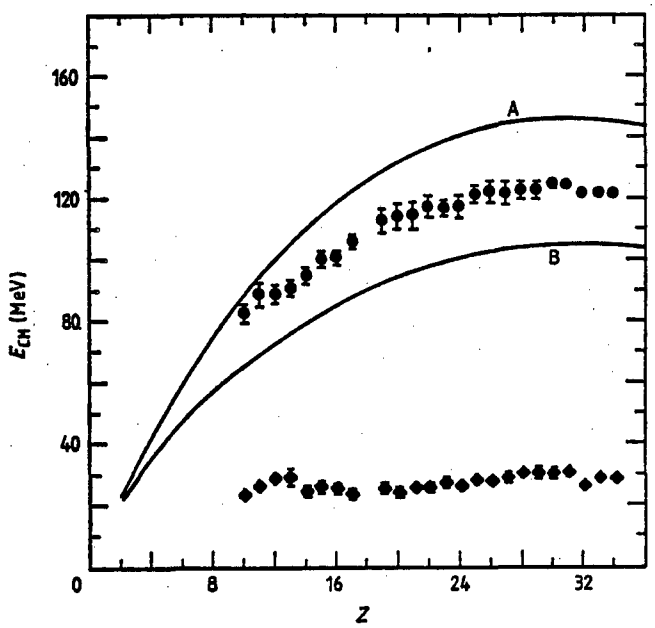

Figure 5. Centroids of the relaxed energy component of the kinetic energy distributions for the reaction ^{197}Au + 288 MeV ^{40}Ar as a function of observed Z. The two full curves are the expected values assuming that the complex consists of two touching spheres (A) and two touching spheroids (B), respectively. ●, $\langle \hat{E}_{CM} \rangle$; ◆, $\langle FWHM \rangle_{CM}$.

identify two distinct components in the energy spectra: a high-energy or quasi-elastic component, and a low-energy or relaxed component. For progressively larger mass transfers either to or from the projectile, the strength of the quasi-elastic component gradually diminishes and eventually disappears altogether. Similarly, as the observation angle is moved away from the grazing angle in either direction, the energy spectra tend to become more and more relaxed. At angles very far from the grazing, the energy spectra consist of just a single Gaussian-shaped relaxed peak.

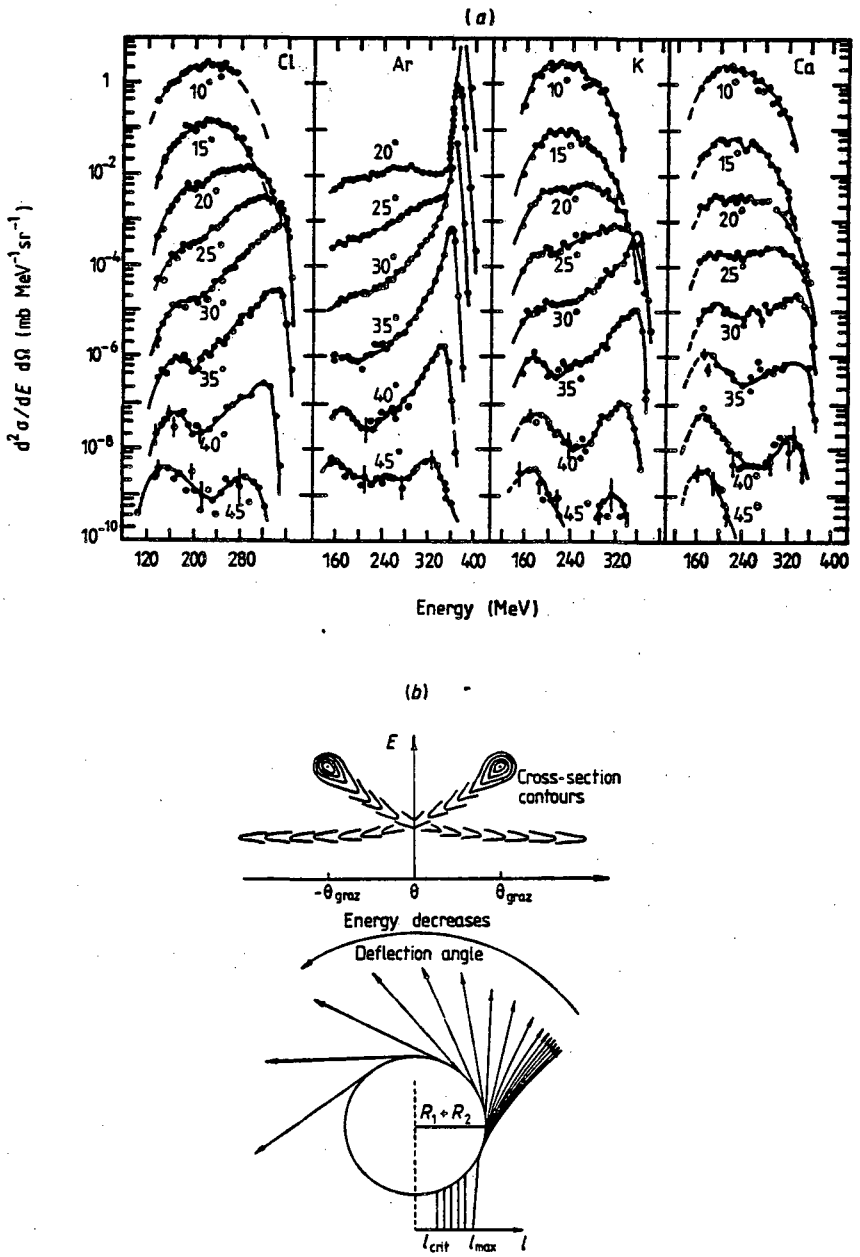

Figure 6. (*a*) Energy spectra for selected elements produced in the $^{232}Th+^{40}Ar$ reaction at various laboratory angles. (*b*) Interpretation of the energy spectra proposed by Wilczynski.

Insight into the variation of the energy spectra with angle and charge transfer can be gained by considering figure 6(*b*). For angular momenta close to the maximum the two nuclei undergo grazing collisions. Because the two nuclei barely overlap the kinetic energies and masses are not altered appreciably, so the nuclei continue along Coulomb-like trajectories. Hence, the yield for these quasi-elastic products are concentrated around the grazing angle. For smaller impact parameters, or lower l waves, more intimate contact is made between the nuclei, leading to stronger damping of the kinetic energy and more extensive mass transfer. In this case, the trajectories are more strongly altered. For a strongly attractive force between the fragments, the trajectories will be pulled in, resulting in scattering towards smaller angles. At still lower impact parameters negative angle scattering and even orbiting can occur. These l waves produce the lower energy ridge in figure 1. For light systems the lowest partial waves can actually become trapped, producing a compound nucleus.

In single-particle inclusive measurements, negative and positive angle scattering are not distinguished. Hence, one expects to observe two overlapping ridges of cross section in agreement with data from Ar+Th and similar reactions. Supportive evidence for the above picture is found in the coincidence measurements involving the circular polarisation of γ-rays emitted by deep inelastic fragments. Positive and negative angle scattering should lead to different spin polarisations of the fragments. Experiments on the reactions Ar+Ag and O+Ni indicate that negative angle scattering does indeed occur (Trautmann *et al* 1977, Lauterbach *et al* 1978).

It should be pointed out that there is nothing sacred about the pattern observed in the Wilcynski plot for the Ar+Th. For very different internuclear potentials, different patterns are observed in the E–θ plane. Consider a Wilczynski plot for the reaction Xe+Bi (see figure 7). In this case the quasi-elastic ridge is vertical rather than oblique (Schröder *et al* 1978). Such behaviour, which is exhibited in reactions involving very heavy ions, is largely due to the strong Coulomb forces which tend to make the inter-

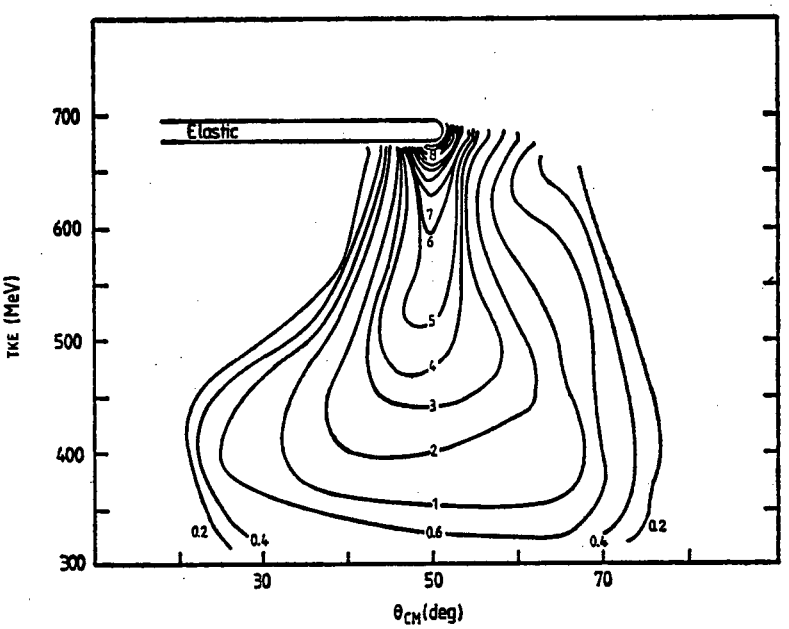

Figure 7. Wilczynski plot for the reaction ^{209}Bi+1130 MeV ^{136}Xe (Schröder *et al* 1978).

nuclear potential repulsive. Hence one applies the phrase 'Coulomb-dominated' to these systems.

4.2. *Nuclear friction*

The 'bare bones' approach to energy dissipation processes is epitomised in classical friction models. In these models one adopts the deterministic point of view of classical mechanics. Due to the neglect of fluctuations, these models are limited to reproducing average values. Despite this limitation, friction models are very popular. In fact, they form the basis for our current understanding of compound-nucleus formation (e.g. Bondorf *et al* 1974, Gross and Kalinowski 1978, Birkelund *et al* 1979).

To build a model of dissipative processes, one needs three ingredients to substitute into the equations of motion: (i) inertial forces, (ii) conservative forces and (iii) dissipative forces. Let us now consider each of these terms.

For large separations, the inertia is just the reduced mass, μ. Generally it is assumed that one can continue to use μ throughout the trajectory even though it is clear that this assumption must break down for large interpenetrations.

The conservative terms arise from centrifugal, electromagnetic and nuclear forces. Given a knowledge of the shape of the system, the first two terms can be dealt with in a relatively straightforward manner. The last term presents more of a problem since the nuclear force is a complicated beast indeed. To make the problem tractable, one generally assumes that the nuclear forces can be derived from a potential which depends only on the separation of the fragments. This potential has been calculated using a variety of approaches, employing both microscopic and macroscopic starting points. Of particular interest is the proximity potential, which is based on replacing the interaction energy associated with two juxtaposed diffuse surfaces by a sum of contributions from parallel surface elements (Blocki *et al* 1977). This approach yields a potential energy of the form

$$V(s)=4\pi\gamma\bar{R}b\Phi(s/b) \tag{4.1}$$

where $\bar{R}$ is a measure of the curvature of the two objects, γ is the surface energy per unit area, b is the width of the diffuse surface, and Φ is a universal function which depends only on the separation of the surfaces, expressed in units of the diffuseness, s/b.

Whatever prescription is employed in calculating the potential, one generally ends up with curves like those shown in figure 8(a). For light systems and for small l values, there is a pocket due to the attractive part of the nuclear potential. As l increases the pocket is 'filled in' by the centrifugal potential. Similarly, increasing the size of the ions increases the Coulomb forces and also destroys the pocket. Hence one sees that only scattering is possible for very heavy systems and for light systems at high angular momenta.

Obviously, the strength of the dissipative forces plays an important role too. The effect of varying the radial friction is illustrated in figure 8(b). Very strong or very weak radial friction results in scattering. In the presence of a moderate frictional force, however, the system can become trapped in the pocket, possibly leading to fusion.

Several forms have been suggested for the frictional forces which are operative in heavy-ion collisions. Using the hydrodynamic analogy, a number of authors (e.g. Tsang 1974, Albrecht and Stocker 1977) have employed the form

$$F=-k\int \mathrm{d}^3x\rho_1(x,r)\,\rho_2(x,r)\,v(x,r) \tag{4.2}$$

where the $\rho_i(x,r)$ are the matter densities of the nuclei at point x when the ions are

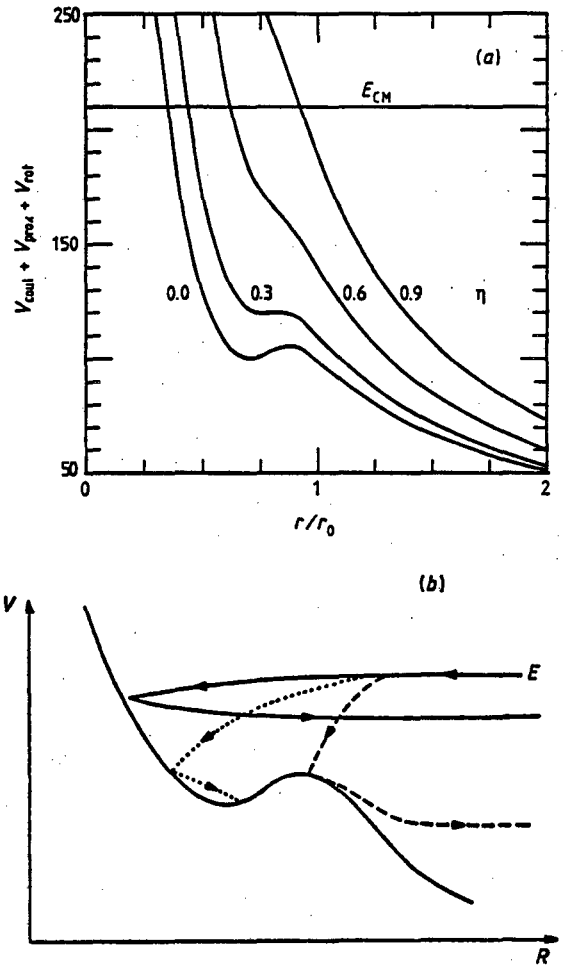

Figure 8. (*a*) Potential energies at a function of r/r_0 for various values of $\eta = l/l_{max}$. (*b*) Schematic showing the trajectories in the presence of weak (full curve), moderate (dotted curve) and strong (broken curve) radial friction (from Schröder and Huizenga 1977).

separated by a distance r, and v is the relative velocity at that point. Equation (4.2) states that the energy is dissipated in the region where the two ions overlap and are moving relative to one another. At the microscopic level equation (4.2) implies that the source of the viscosity is nucleon–nucleon collisions, and is an example of what has come to be called two-body dissipation.

For a two-body dissipation mechanism to be effective, the mean free path of the nucleons must be short compared to the dimensions of the interaction region. However, the success of mean field theories like the shell model has taught us that the mean free path is actually long due to the Pauli principle, which prevents scattering into occupied levels. In the spirit of the mean field theories a nuclear one-body dissipation mechanism has been proposed (Blocki *et al* 1978) in which the energy damping occurs via inelastic collisions of the individual nucleons with the time-dependent average single-particle potential. Randrup (1978) has shown that the Rayleigh dissipation function for one-body proximity friction is given by

$$F = \pi n_0 R b \Psi(s/b)\,(2v_r^2 + v_t^2) \tag{4.3}$$

where v_r and v_t are, respectively, the radial and tangential velocities, n_0 is the bulk flux of nucleons within the nucleus ($\approx 2.5 \times 10^{-23}$ MeV s fm^{-4}), and Ψ is a universal function which depends on the separation expressed in units of the surface thickness b. The analogy between equations (4.1) and (4.3) is readily apparent.

Another energy dissipation mechanism has been proposed by Broglia and co-workers (Broglia *et al* 1976, 1979). In contrast to the mechanisms mentioned above which rely on the assumption that the response time for the nucleonic degrees of freedom is short compared with that of collective modes, Broglia has argued that the relative motion may be strongly coupled with other collective modes, like giant resonances. Damping of these modes then converts the collective energy into intrinsic excitation of the fragments. A number of experimental studies (Frascaria *et al* 1977, 1980) have revealed a number of structures in the kinetic energy spectra (see figure 9). It has been suggested that these structures might be due to giant resonances; however, other explanations have been offered. Until alternative explanations, like the emission of light particles (Hilscher *et al* 1979), have been ruled out, one must reserve judgement on the matter.

Although it is not yet clear which (if any) of the three mechanisms considered above plays the dominant role in the energy dissipation process, it is certainly clear from the low kinetic energies of the fragments that shape deformations are important at least in the final stages of the reaction. By including shape degrees of freedom in friction models, one can reproduce the final kinetic energies with reasonable success (e.g. Deubler and Dietrich 1975, Siwek-Wilczynska and Wilczynski 1976). Moreover, shape degrees of

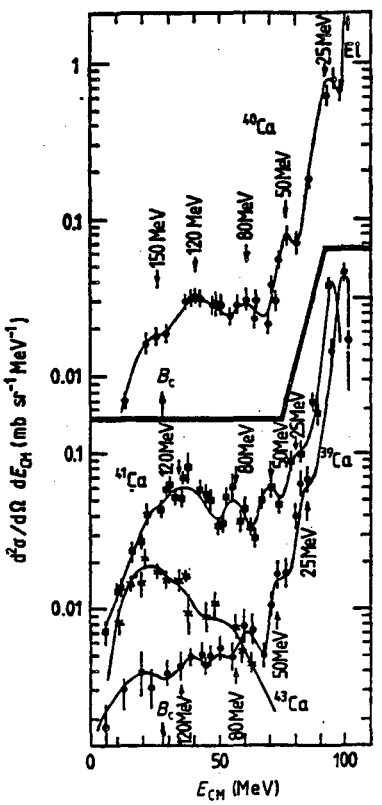

Figure 9. Centre-of-mass energy spectra for Ca isotopes produced in the ^{40}Ca+400 MeV ^{40}Ca reaction at 10° in the laboratory system. Arrows indicate the positions of structures which might be due to the excitation of giant resonances (Frascaria *et al* 1980).

freedom also provide a mechanism for producing fluctuations in the kinetic energy, i.e. a system in contact with the heat reservoir provided by the internal degrees of freedom can undergo shape fluctuations by drawing energy out of the reservoir and investing it in an energetically less favourable shape (Moretto 1975).

Wolschin (1979) has taken a more general approach to the problem utilising transport theory. In his shape relaxation model, the initially spherical fragments gradually deform towards their equilibrium deformations. At the same time, the heat bath provided by the dissipated kinetic energy allows the deformations to fluctuate. Reasonable agreement with experiment is achieved in this treatment (see figure 10).

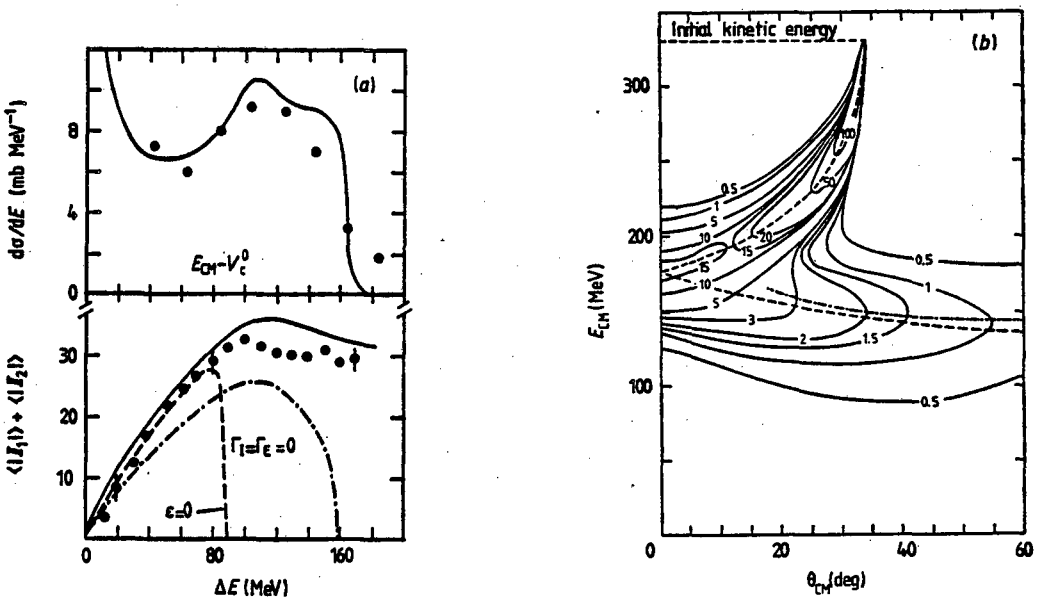

Figure 10. (*a*) Calculated energy spectrum and angular momentum distribution in comparison with the data of Olmi *et al* (1978) for 5.99 MeV AMU^{-1} ^{86}Kr+^{166}Er. The mean absolute value of the intrinsic angular momentum has been deduced from the measured γ-multiplicity. Calculated curves are without consideration of deformation and fluctuations (broken), including deformation (chain) and including both deformation and angular momentum plus energy fluctuations (full). (*b*) Calculated Wilczynski plot for the reaction ^{232}Th+388 MeV ^{40}Ar. Broken curve is the centroid of the ridge obtained from figure 1. The chain curve is the centroid of the calculated result.

Fluctuations about these mean values of any collective degree of freedom can also be considered within the framework of transport theory. As an example, a calculation for the Ar+Th reaction is shown in figure 10 (Berlanger *et al* 1978). Clearly the general features of the experimental Wilczynski plot are well reproduced.

4.3. The fate of the dissipated energy

Although it is apparent from the energy spectra that a very large fraction of the entrance channel kinetic energy can be dissipated, the fate of this 'lost' energy is not so obvious. By analogy to other systems in which dissipative forces are operative, one suspects that much of the damped energy might be converted into thermal excitation. However, since the time scale for the energy dissipation process appears to be short, in fact uncomfortably

close to the nucleonic time scale, other scenarios such as prompt particle emission are not easily ruled out.

Thus, it is rather surprising to note that a variety of experiments have shown that the dissipated energy is largely thermalised even at high bombarding energies. This has been demonstrated in the study of the reactions ^{63}Cu+158,252 and 343 MeV ^{20}Ne (Schmitt *et al* 1978). In light systems like this one, the de-excitation of the fragments is dominated by the emission of light charged particles. This feature was exploited in the experiments by simultaneously measuring the atomic numbers of the two heavy fragments. In figure 11 the missing charge ΔZ is plotted against the kinetic energy and the available excitation energy as inferred from the kinetic energies. Although the ΔZ varies dramatically with bombarding energy, it is a linear function of the excitation energy. The slope is approximately 25 MeV/ΔZ. Since one expects that the total mass loss should be approximately twice the missing charge, this slope implies an energy loss of about 12.5 MeV/AMU, which is consistent with energy thermalisation.

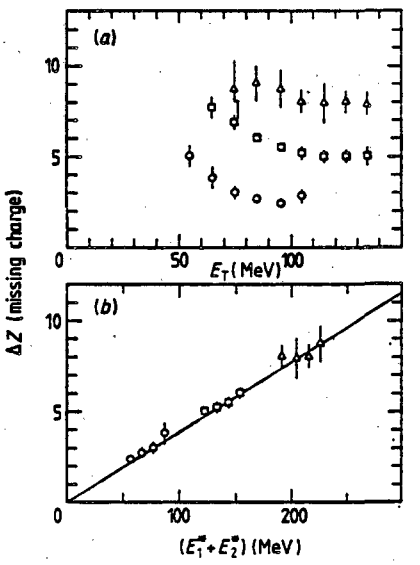

Figure 11. (*a*) Missing charge plotted against total exit channel kinetic energy for various bombarding energies in the reaction ^{20}Ne+^{63}Cu. ○, $\theta=50°$, $E=158$ MeV; □, $\theta=42°$, $E=252$ MeV; △, $\theta=38°$, $E=343$ MeV. (*b*) Missing charge plotted against excitation energy.

Even though the dissipated energy appears to be largely thermalised, this does not imply that the two fragments are in thermal equilibrium. For a given mass asymmetry the excitation energy can be divided between the fragments in a variety of ways as dictated by the product of the level densities of the fragments:

$$P(x)\,\mathrm{d}x \propto \rho_1(x)\,\rho_2(E^*-x)\,\mathrm{d}x.$$

The quantity $\ln P(x)$ is readily identified with the total entropy of the system. At equilibrium a necessary condition is

$$\frac{\mathrm{d}\ln P(x)}{\mathrm{d}x}=0=\frac{\mathrm{d}\ln \rho_1(x)}{\mathrm{d}x}+\frac{\mathrm{d}\ln \rho_2(x)}{\mathrm{d}x}=\frac{1}{T_1}-\frac{1}{T_2}$$

where T_1, T_2 are the thermodynamic temperatures of the two fragments. In the Fermi gas model, the excitation energy is related to the temperature by $E^*=aT^2$ where a is the

level density parameter. For a broad range of masses and excitation energies, $a \cong A/8$ where A is the fragment mass. Hence it is easily seen that the equilibrium condition $T_1 = T_2$ implies that the excitation energy is divided according to the mass ratio of the fragments. The question of energy equilibration has been explored in two types of experiments: heavy-ion–heavy-ion coincidence studies and heavy-ion–light-particle studies.

The basis of the former technique (Gelbke *et al* 1976, Babinet *et al* 1978, Cauvin *et al* 1978) is largely kinematical. For a purely binary process, conservation of linear momentum can be expressed in the laboratory system as

$$A_j E_j = A_1 E_1 \frac{\sin^2 \theta_k}{\sin^2(\theta_3 + \theta_4)} \begin{cases} j=3 & \text{and} \quad k=4 \\ \text{or } j=4 & \text{and} \quad k=3 \end{cases} \tag{4.4}$$

where the subscript 1 refers to the projectile and the subscripts 3, 4 refer to the reaction products. The symbols E and θ denote the laboratory energies and angles, respectively. Obviously the emission of light particles will alter the energies and angles of the fragments from their initial values. For an evaporation process the average final fragment energies, E_j', are approximately

$$E_j' = E_j(1 - \nu_j/A_j)$$

where ν_j is the number of nucleons lost in the decay. The angles in equation (4.4) can be replaced by the average experimental values for a large number of events without introducing any appreciable error.

Using the above equations together with conservation of nucleon number, $A_1 + A_2 = A_3 + A_4$, one can determine the pre-evaporative mass of the fragments and the total number of evaporated mass $\nu_3 + \nu_4$. Conservation of energy provides another equation allowing one to extract ν_3 and ν_4 separately.

Results from the study on $^{58}Ni + ^{40}Ar$ (Babinet *et al* 1978) are shown in figure 12. The average number of evaporated nucleons is plotted against the atomic number of the light fragment. Since Z_3 is approximately proportional to A_3, the linear increase implies that the excitation energy is divided according to the mass ratio of the fragments. This is further supported by the very good agreement between experiment and evaporation calculations which are based on this assumption (Cauvin *et al* 1978).

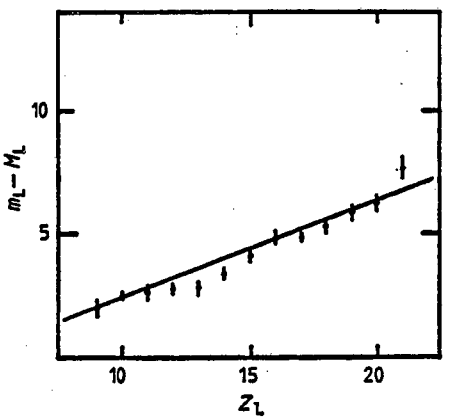

Figure 12. Number of evaporated neutrons plotted against the atomic number of the fragment prior to evaporation for the $^{58}Ni + ^{40}Ar$ reaction.

Results from a direct measurement of neutrons emitted in the reaction ^{197}Au+ 400 MeV ^{63}Cu are shown in figure 13 (Tamain *et al* 1979). These data and others like them (Eyal *et al* 1978, Hilscher *et al* 1979, Gould *et al* 1980) verify directly that the energy is indeed split according to the masses and that the fragments have equal temperatures (since the slopes of the energy spectra are equal). Moreover, these neutron experiments have shown that this energy partition occurs not only for completely relaxed events, but also for the whole range of Q values up to very small energy losses.

Although experiments described in the preceding paragraph have shown little evidence for non-thermal decay of the primary fragments, a number of α-particle–heavy-fragment coincidence experiments have been interpreted in terms of a sometimes large probability for prompt α-emission (e.g. Harris *et al* 1977, Hò *et al* 1977, Gelbke *et al* 1977, Gamp

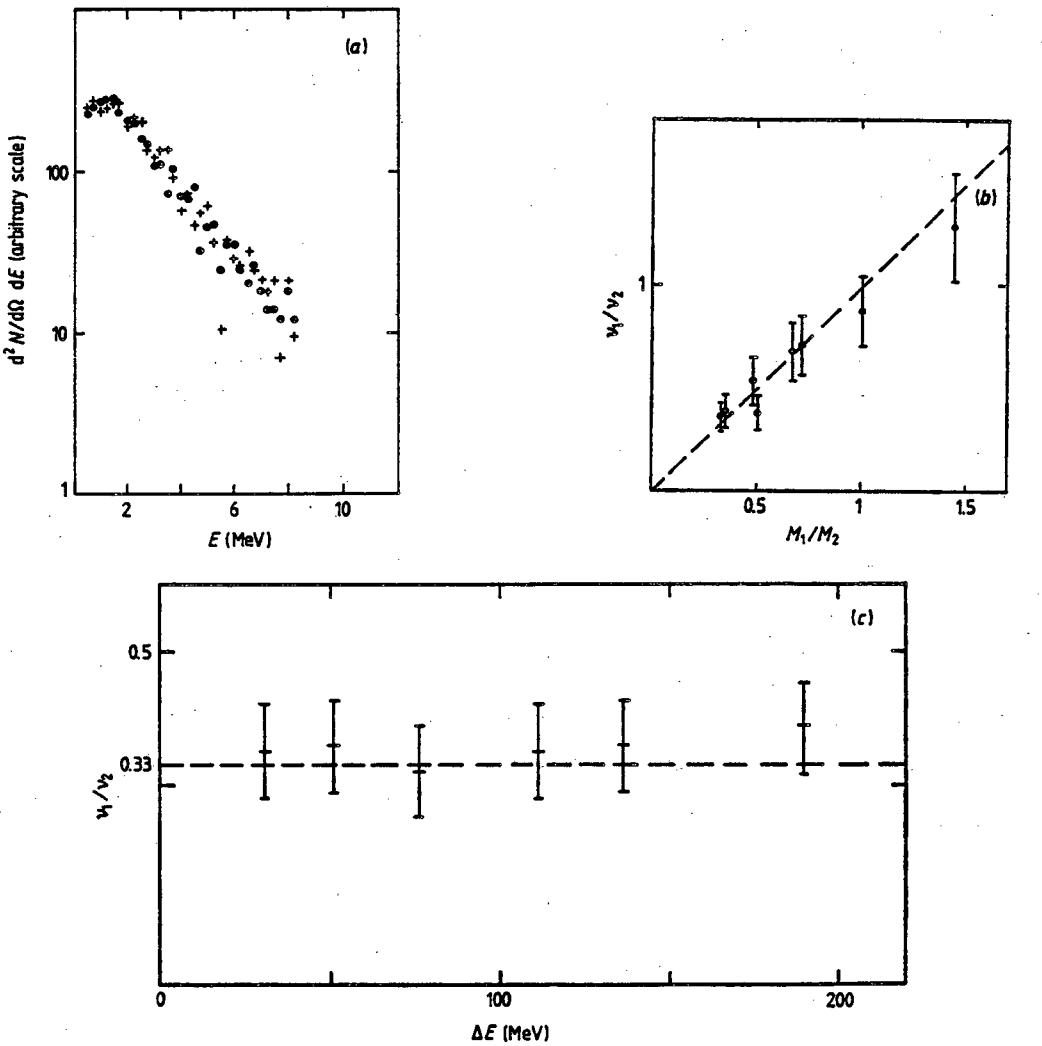

Figure 13. (*a*) Centre-of-mass kinetic energy spectra of the neutrons associated with the two fragments in the Cu+Au reaction. ●, detected fragment at 40°; +, detected fragment at 63°. (*b*) Ratio between the number of neutrons emitted by the two fragments plotted against the mass ratio of the two fragments in the reaction 400 MeV Cu+Au. ○, detected fragment; ●, partner fragment. (*c*) Ratio of the mean number of neutrons emitted by the two fragments ν_1/ν_2 plotted against the mean kinetic energy loss for the Cu+Au reaction.

et al 1978, Bhowmik *et al* 1978, Miller *et al* 1978). These so-called pre-equilibrium α-particles are frequently (but not always) focused at small angles, i.e. along the beam direction, and often have energies substantially higher than those expected for evaporation from equilibrated fragments.

These experimental observations have prompted theorists to suggest a number of mechanisms. One possibility is that a 'hot spot' (Bethe 1938) is produced in the region of contact between the two heavy ions (Weiner and Weström 1975, Gottschalk and Weström 1977, Nomura *et al* 1978). Such a hot zone could be produced in the presence of strong two-body viscosity. Another possible mechanism which has been advanced is the Fermi jet (Robel 1979) or the PEP jet (Bondorf *et al* 1980). In contrast to the hot spot model, this mechanism starts with one-body viscosity: the fast particles are produced via the coupling of the relative motion to the Fermi motion within the nuclei.

Thus far no experiment has provided a clear signature of the production mechanism for prompt particles. In fact, it is fair to say that the conditions for fast particle emission in deep inelastic heavy-ion collisions at energies $\leqslant 20$ MeV/nucleon are poorly understood. Perhaps when we do achieve a reasonable understanding of these phenomena we will at the same time establish the dominant mechanism for the energy loss process.

5. The mass asymmetry mode

5.1. The ridge line revisited

As discussed earlier, the charge distributions at equilibrium should be of the form

$$Y(Z) \propto \exp(-V(Z)/T) \tag{5.1}$$

where T is the nuclear temperature and V is the potential energy as a function of charge asymmetry, or ridge line potential energy (Moretto 1975). Despite the fact that the mass asymmetry degree of freedom is usually far from equilibrated in heavy-ion reactions, it frequently plays an important role in determining the shape of the charge and mass distributions. In fact, with some knowledge of $V(Z)$ and a rough idea of the interaction time one can often explain the general features of the charge distributions.

In order to calculate the ridge line potential one must resort to a model. Because of its simplicity and proven success in reproducing macroscopic nuclear properties, we will use the liquid drop model. Within the framework of the liquid drop model, the potential energy as a function of the Z of one fragment is

$$V(Z_1, Z_T) = V_{LD}(Z_1) + V_{LD}(Z_T - Z_1) + V_{int} + V_{rot}(l)$$

where l is the total angular momentum, V_{LD} is the liquid drop (i.e. surface+Coulomb) energy of a fragment, V_{int} is the interaction energy, and V_{rot} is rotational energy. To calculate $V(Z_1, Z_T)$ it is necessary to make some assumptions concerning the geometry of the di-nuclear intermediate complex. For simplicity we shall assume that the complex consists of two touching spheres.

A number of general topological features of the ridge line potential are illustrated by calculations for the systems N+Ag and Kr+Au (see figures 14 and 4, respectively). For low values of the angular momentum, light systems like N+Ag exhibit a maximum in the potential energy at symmetry, whereas heavy systems like Kr+Au display a local minimum at symmetry. However, at sufficiently high l values the potential energy always possesses a local minimum at symmetry. As the calculations for Kr+Au show,

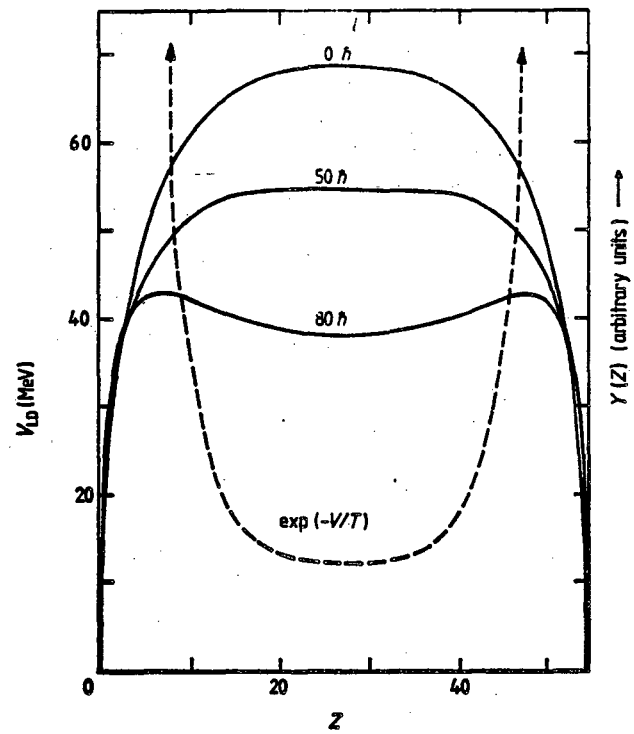

Figure 14. Liquid drop potential energy of two touching spheres for N+Ag for various values of the angular momentum. The broken curve displays the expected yield distribution for the $l=50\hbar$ curve, assuming that the temperature of the complex is 3 MeV.

the depth of this minimum increases with l. The local maxima which flank this minima at symmetry are sometimes referred to as the Businaro–Gallone mountains (1955).

In light of equation (5.1) the equilibrium mass or charge distributions for light systems at low angular momentum are expected to be asymmetric. This is illustrated by the broken curve in figure 14. At higher l values symmetric decay will become progressively more important. On the other hand, the equilibrium mass distributions for heavy systems should always peak at symmetry. Obviously, one should be cautious in applying these predictions to heavy-ion reactions since the mass asymmetry mode relaxes very slowly.

5.2. Lifetime regimes of the mass distributions

Like the energy spectra the charge distributions of the fragments produced in heavy-ion collisions attest to a broad range of interaction times. Consider for example the reaction Kr+Au (see figure 4). Two components are discernible in these charge distributions: (i) a quasi-elastic component which is strongly peaked at the projectile atomic number and is visible in the angular region around the grazing angle (about 40°), and (ii) a much broader relaxed component which is visible throughout the entire angular range. In so far as the breadth of the charge distribution is reflective of the interaction time, one can associate the narrow (quasi-elastic) component with short interaction times and the broader (relaxed) component with long interaction times.

A more striking illustration of the great variety of interaction times is apparent from a comparison (figures 4 and 15) of the Kr+Au charge distributions with those observed

for the reaction Ne+Ag (Babinet *et al* 1976). Except at forward angles where contributions from partially damped processes are in evidence, the charge distributions for Ne+Ag are very broad. Thus it appears that in the Kr+Au reaction the mass asymmetry mode is far from equilibrated while in the case of Ne+Ag the mass asymmetry mode is close to equilibrium (that equilibrium is not fully achieved in the latter system will become apparent in the next section).

A comparison of data from a wide variety of heavy-ion reaction studies shows that many of the charge distributions can be assigned to one of two categories: (i) the short-lifetime regime (narrow charge distributions like Kr+Au); or (ii) the long-lifetime regime (broad distributions like Ne+Ag). Most of the short-lifetime systems which have been studied have involved massive projectiles like Cu, Kr, Xe while most of the long-lifetime systems are associated with relatively light projectiles like Ne and Ar. Hence it is not surprising that early investigators suggested that the lifetime regime was

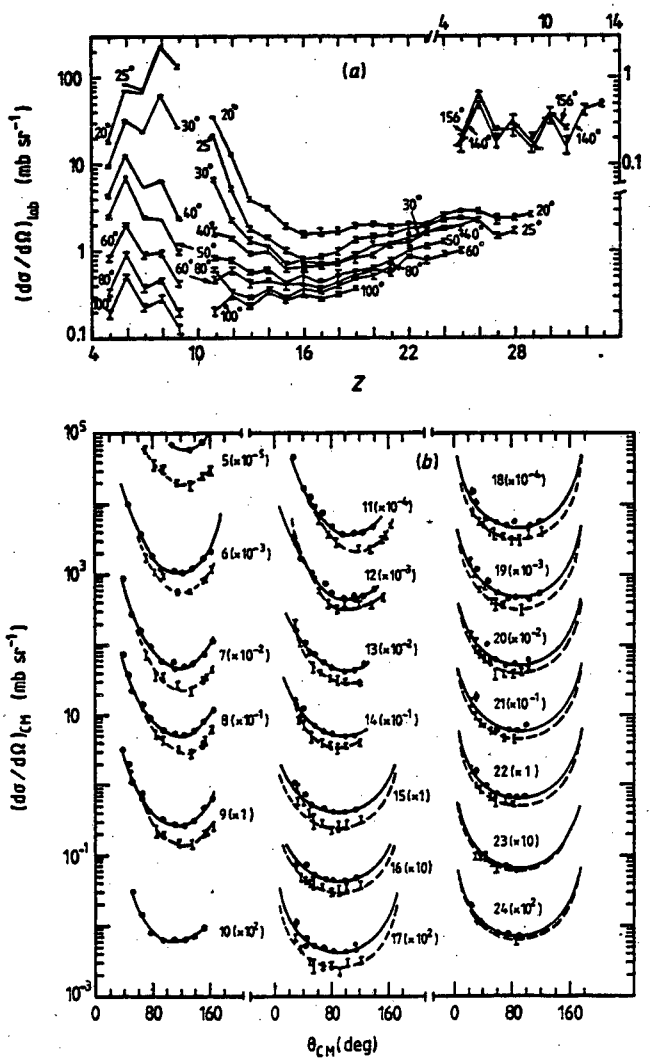

Figure 15. (*a*) Laboratory charge distributions for the reaction ^{nat}Ag+175 MeV ^{20}Ne. (*b*) Angular distributions in the centre of mass for the various Z given on each set of curves in the reactions 175 MeV (I) and 252 MeV (Φ) ^{20}Ne+^{nat}Ag.

determined by the masses of the heavy ions. That this is not the case was demonstrated in studies in which both kinds of charge distributions were produced for the same target–projectile combination (Moretto and Schmitt 1976, Mathews *et al* 1977, Agarwal *et al* 1977, Rivet *et al* 1977) by varying the ratio of the centre-of-mass kinetic energy to the interaction barrier, E/B. For values of $E/B < 1.5$, the charge distributions are narrow and are peaked in the vicinity of the projectile. For larger values of E/B, the distributions are broader and show substantial drifts in their centroids.

While the widths of the charge distributions give some indication of the interaction time, the most direct handle on the time scale is the angular deflection of the fragments. For interaction times which are short compared to the rotational period, the system

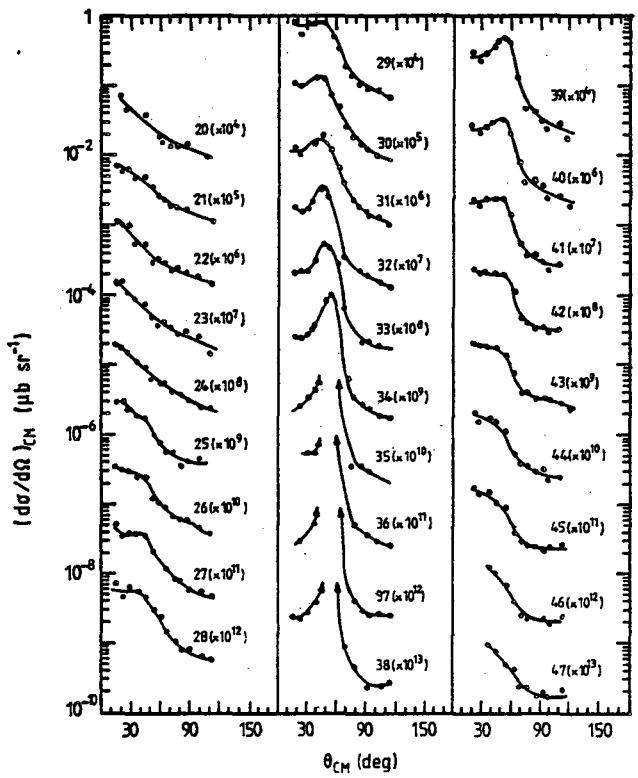

Figure 16. Centre-of-mass angular distributions for the reaction ^{197}Au + 620 MeV ^{86}Kr for atomic numbers 20–47, given for each curve.

barely rotates before it decays, leading to angular distributions which are peaked on the side of impact. For longer lifetimes the system can undergo larger angular deflections, leading to angular distributions which are forward-peaked. If the interaction time is comparable to or larger than the rotational period of the di-nuclear system, the centre-of-mass angular distributions will tend towards $1/\sin\theta$ (Ericson 1960).

In figures 15 and 16 the angular distributions as a function of fragment charge are shown for the systems Ne + Ag and Kr + Au. Note that the characteristics of the angular distributions are in accord with our observation about the widths of the charge distributions. The angular distributions for the system Kr + Au, which displays narrow charge distributions, are extensively side-peaked, whereas the angular distributions for the Ne + Ag system, which exhibits broad Z distributions, are largely forward-peaked.

5.3. Evidence for diffusive evolution of the mass asymmetry

Insight into the mechanism of the mass transfer process can be gained by a closer examination of the angular distributions as a function of Z. Let us first consider the short-lifetime regime as exemplified by the reactions Kr+Au (figure 16). The angular distributions for elements with atomic numbers close to that of the projectile are strongly side-peaked. As the atomic number of the fragment is increased or decreased with respect to the projectile Z, the peak in the angular distribution gradually moves toward smaller angles, first producing a shoulder for intermediate charge transfer and eventually disappearing, leading to forward-peaked angular distributions for the largest transfers.

The pattern of the angular distributions suggests that small net charge transfers to or from the projectile are associated with short interaction times while larger net transfers are associated with progressively longer interaction times. These observations are readily explained in terms of a diffusive evolution of the mass asymmetry mode. For a diffusive mechanism the spread in the mass distribution increases with time; therefore, the time delay in populating a particular Z in the exit channel should increase as the quantity $|Z-Z_{\mathrm{proj}}|$ increases. Thus the time delay associated with larger and larger charge transfers can be correlated with the continuous transition from side-peaked to forward-peaked angular distributions.

The patterns of the charge and angular distributions for long-lifetime regime systems are more diverse. Let us consider two systems with similar total A and Z: Ne+Ag and Ar+Ni (Gatty *et al* 1975). For the reaction Ne+Ag one observes a minimum in the cross section at about $Z=15$, a rapid increase in the cross section at lower Z values, and a weak increase at higher Z values. In contrast the pattern for the Ar+Ni reaction (see figure 17) is radically different: the yield increases steadily with increasing Z until it reaches a maximum at symmetry.

These differences can be explained in terms of a diffusive evolution of the mass asymmetry along the ridge line. Let us see how this comes about. For the Ne+Ag reaction the entrance channel asymmetry, or injection point, will lie to the left of the Businaro–Gallone mountains for a large number of l waves. Consequently, as the mass asymmetry begins to evolve, the system will be rapidly pushed towards more asymmetric configurations. In contrast, for Ar+Ni the potential energy in the vicinity of the injection point, which is near symmetry, exhibits a minimum. Hence for most l waves the system is trapped in the valley between the Businaro–Gallone mountains.

The angular distributions as a function of charge support this interpretation (see figures 15 and 17). For Ne+Ag the reaction products close to the entrance channel are strongly forward-peaked, indicating that they are produced on a short time scale. This forward peaking persists for elements with Z values smaller than the projectile, indicating that the population of these exit channels also occurs very rapidly. In contrast, the forward peaking of the angular distributions diminishes very rapidly for progressively larger transfers to the projectile. After the transfer of only about four Z units, the forward peaking has vanished and the angular distributions are essentially $1/\sin\theta$. The interpretation of the Ar+Ni angular distributions proceeds along similar lines. (Note that for Ar+Ni the quantity $\mathrm{d}\sigma/\mathrm{d}\theta$ has been plotted rather than $\mathrm{d}\sigma/\mathrm{d}\Omega$; a $1/\sin\theta$ angular distribution appears as a horizontal line when in terms of $\mathrm{d}\sigma/\mathrm{d}\theta$.) For Ar+Ni one again observes strong forward peaking close to the projectile atomic number due to the short average interaction time. As the charge of the fragment decreases, the angular distributions gradually evolve toward the long-lifetime limit indicating an increasing time delay associated with the production of these products.

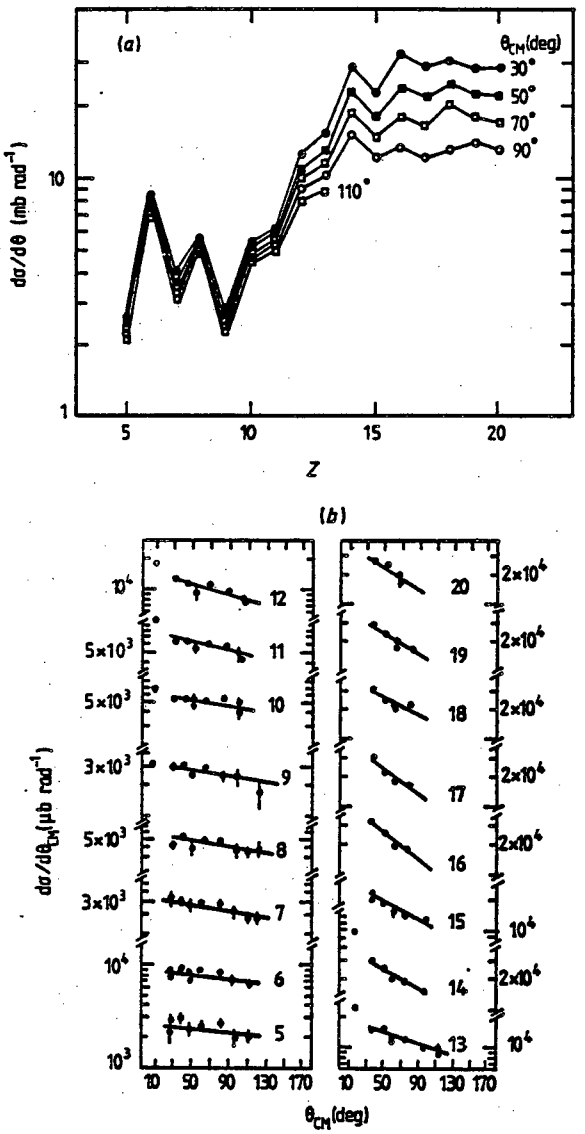

Figure 17. (*a*) Centre-of-mass charge distributions at various angles for the reaction ^{58}Ni + 280 MeV ^{40}Ar. (*b*) Centre-of-mass charge distributions at various angles for the reaction ^{58}Ni + 280 MeV ^{40}Ar for various Z values given for each curve. Note that the quantity $d\sigma/d\theta$ ($=2\pi \sin\theta\, d\sigma/d\Omega$) is plotted on the vertical axis.

5.4. Applications of transport theory

In view of the myriad of transport models which have been applied to deep inelastic reactions, it is impractical to make a really extensive comparison with experiment. Instead we shall focus on a single approach employing the Fokker–Planck equation. Though simple, this approach nicely illustrates most of the important physics.

For heavy systems and for asymmetries between the Businaro–Gallone mountains, the ridge line potential is approximately parabolic for a broad range of angular momenta. Thus one can readily make use of the analytical solution of the Fokker–Planck equation to calculate the charge distribution $\varphi(Z, t)$.

Both the ridge line potential energy and the diffusion rate, which enters through the quantity K (see equation (3.6)), depend on the interpenetration of the fragments and their shapes. Furthermore, calculation of the interaction time t requires knowledge of the dynamics. In the absence of detailed information concerning the time evolution of the system, we shall limit ourselves to an extremely simplistic approach which nevertheless closely respects the experimental data (Moretto 1978).

Let us first assume that the time-dependent curvature of the ridge potential can be replaced by a time-independent quantity which reflects the average shape of the system. Since we know that a ridge potential for interpenetrating spheres can qualitatively explain many of the experimental features, we shall make this assumption. The curvature is then easily obtained from a parabolic fit to the ridge line potential as calculated from the liquid drop model.

The diffusion rate can be obtained from the work of Randrup (1978):

$$\kappa f = 2\pi n_0 R b \Psi(\zeta)$$

where n_0 is the particle flux in nuclear matter at its saturation density (2.5×10^{-23} MeV s fm^{-4}), $\bar{R}=C_1C_2\,(C_1+C_2)^{-1}$ is the reduced radius of the system expressed in terms of the central radius (C_1 and C_2) of the two fragments, b ($\cong 1$ fm) is the skin thickness, and the quantity $\Psi(\zeta)$ is a universal function which depends only on the separation between the sharp surfaces of the fragments expressed in units of the skin thickness. This approach neatly factors out the geometrical features of the problem.

The radial potential can be written as

$$V(D)=V_{\text{prox}}+\frac{Z(Z_T-Z)\,e^2}{D}+\frac{\hbar^2 l^2}{2\mathscr{I}(l)} \tag{5.2}$$

$\mathscr{I}(l)$ being the appropriate moment of inertia.

It is not very clear how much the fragments must interpenetrate before the above equation breaks down. This makes it difficult to formulate the dynamical problem. We shall just use the above potential to calculate the average force $F_R(l)$ at the interaction distance D_{int}: $F_R(l)=\partial V(D)/\partial D|_{D_{\text{int}}}$. From the knowledge of the reduced mass μ, the radial velocity v_R, and the radial force F_R for each l value at the interaction radius, one can introduce the following two ansatz for the interaction time t and the average interpenetration x of the fragments:

$$t(l)=\frac{2\mu v_R}{F_R}=\frac{2[2\mu(E-B)]^{1/2}}{F_R}\left(1-\frac{l^2}{l_{\max}^2}\right)^{1/2} \qquad \bar{x}(l)=\frac{\alpha}{2}\frac{\mu v_R^2}{F_R}. \tag{5.3}$$

In a more serious attempt to fit the experimental data one could resort to a more detailed dynamical calculation. Obviously, it is a trivial matter to substitute the ansatz in equation (5.3) with more reliable expressions. The diffusion along the asymmetry coordinate is then allowed to proceed with a form factor dependent upon $\bar{x}(l)$ for a time $t(l)$.

The tangential motion is treated assuming for the equation of motion the simple form:

$$F_T=\mu\gamma(\omega_0-\omega_{\text{rig}}) \tag{5.4}$$

where ω_0 and ω_{rig} are the two limiting orbital angular velocities corresponding to sliding and sticking. The constant γ is chosen to approximately reproduce the mean kinetic energies as a function of angle, assuming that all of the radial energy is lost.

The interaction times calculated for the reaction Au+Kr at three energies are shown in figure 18(*a*) as a function of angular momentum. There is good experimental evidence for the angular momentum dependence predicted by our ansatz. It is interesting to notice the rather mild increase in the average lifetime with increasing bombarding energy. The average deflection function is also shown in figure 18(*a*). Notice the well-pronounced deep inelastic rainbow which moves from positive to negative angles as the bombarding energy increases. The 600 MeV curve predicts a rainbow angle of about 50° in excellent agreement with experiment. The movement of the rainbow angle towards smaller and eventually negative angles results from the combination

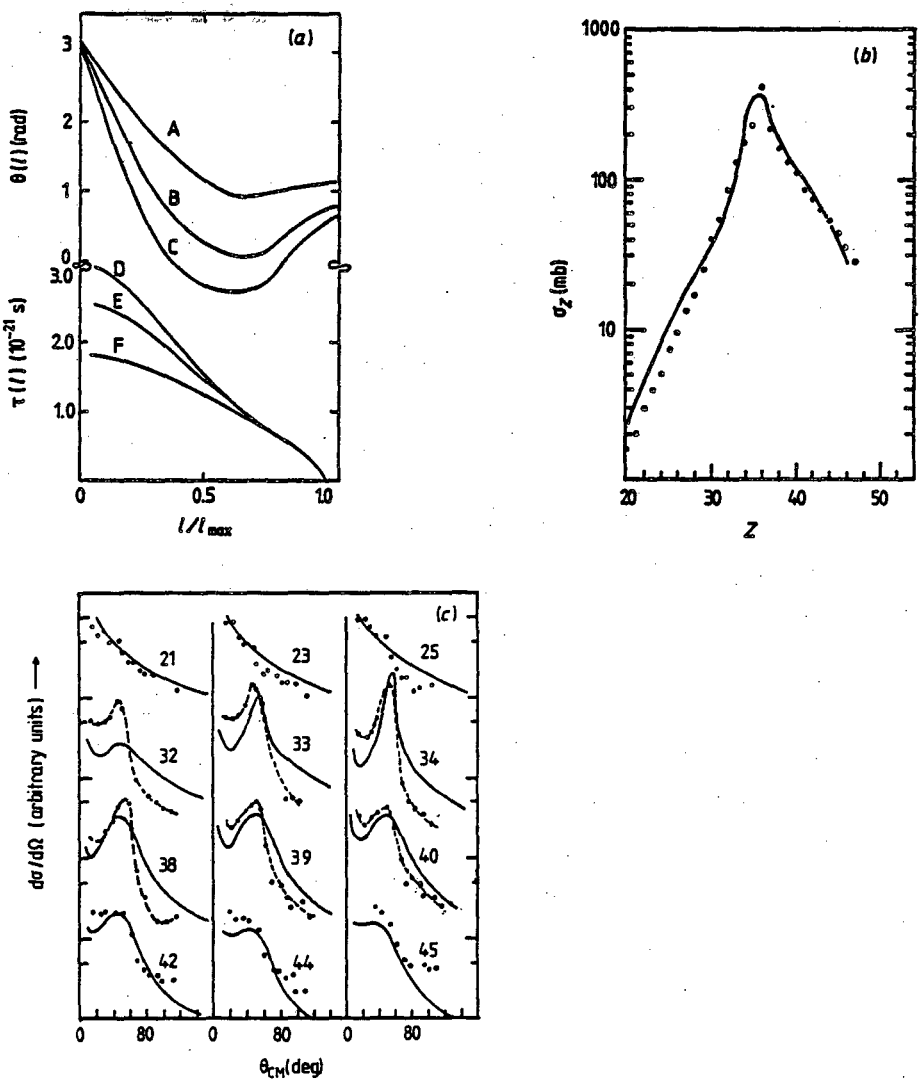

Figure 18. (*a*) Calculated deflection functions (A, 600 MeV; B, 800 MeV; C, 1000 MeV) and interaction times (D, 1000 MeV; E, 800 MeV; F, 600 MeV) for the reaction ^{197}Au+^{86}Kr at various bombarding energies. (*b*) Calculated (full curve) and experimental (points) angle-integrated charge distributions for the ^{197}Au+^{86}Kr reaction. (*c*) Calculated (full curves) and experimental (points) CM angular distributions for the ^{197}Au+^{86}Kr reaction for selected atomic numbers given on each curve. The broken curves are to guide the eye.

of three factors: (i) increasing lifetime, (ii) increasing angular momentum, (iii) decreasing average moment of inertia due to the increasing average penetration.

At this point the cross section can be calculated as a function of exit channel asymmetry for each l wave. Summing over l waves yields the angle-integrated charge distribution. In figure 18(*b*) the calculated angle-integrated Z distributions are compared with experiment for the reaction Au+Kr at 620 MeV. The agreement is reasonable over more than two orders of magnitude. Some of the apparent discrepancies arise from the fact that the experimental angular distributions have been integrated over an incomplete angular range.

A fortiori, the angular distributions can be calculated from the angular deflections of the fragments during the interaction and from their deflection in the Coulomb field. Angular distributions for the Kr+Au are shown in figure 18(*c*). The theory nicely tracks the experiment in predicting forward-peaked angular distributions at small Z which develop into side-peaked angular distributions close to the projectile. For Z above the projectile, the angular distributions slowly lose their side peak and become forward-peaked. The satisfactory agreement with both the Z distribution and the angular distribution shows that the calculated dependence of the interaction times and of the diffusion constant upon angular momentum and radial velocity is reasonably good. Even better agreement can be obtained with a more realistic treatment of the dynamics.

5.5. Long-lifetime components

In addition to deep inelastic reactions, many experimental mass and charge distributions show another component which is peaked at symmetry (e.g. Plasil *et al* 1966, Britt *et al* 1976, Otto *et al* 1976, Oeschler *et al* 1979, Lebrun *et al* 1979). Because this latter component is often apparent in reactions in which complete fusion is also an important process, it has generally been attributed to the fission of a compound nucleus, and is thus referred to as fusion–fission. The kinetic energies and angular distributions of the fusion–fission fragments are also consistent with this interpretation. The former correspond to the Coulomb repulsion energies for touching fragments while the latter are essentially $1/\sin\theta$.

From previous discussions of the characteristics of deep inelastic reactions it should be apparent that the identification of the symmetric component with compound-nucleus fission is not conclusive. For all but very light systems, the ridge line potential energy possesses a minimum at symmetry. Thus for relatively long lifetimes ($\cong 60\times 10^{-22}$ s) deep inelastic processes will also yield mass distributions which peak at symmetry. Furthermore, the kinetic energies for fully relaxed deep inelastic products are essentially indistinguishable from those observed in fission (as far as we know). Lastly, for lifetimes somewhat larger than a rotational period, the angular distributions of deep inelastic fragments are also $1/\sin\theta$.

While this latter scenario, that of a long-lived deep inelastic reaction, may seem rather speculative, there is growing experimental evidence that such a process does indeed exist. Early evidence for this mechanism is found in studies of the reaction ^{197}Au+^{40}Ar. The compound nucleus formed in this reaction (if it is actually formed at all) is ^{237}Bk. Only for low l values would this nucleus have a non-vanishing fission barrier. At higher angular momentum the compound nucleus simply does not exist (Cohen *et al* 1974). Thus, purely on the basis of statics, one concludes that only a fraction of the reaction cross section could be accurately called compound-nucleus fission. Contrary to these

expectations the experimental charge distributions show a large cross section for the 'fusion–fission' process, implying the existence of another reaction mechanism which does not proceed via the formation of a compound nucleus. More recent evidence comes from the work of Heusch *et al* (1978) who studied the reaction Xe+Fe. Their findings show that the charge distributions for this reaction are also difficult to explain with either the fission of a compound nucleus or with standard diffusion model treatments.

Recently systematic surveys of the 'fusion–fission' component have been made by Lebrun *et al* (1979). In these studies a number of composite systems have been prepared with different angular moment by employing different entrance channels. They have observed that the symmetric component persists even at angular momenta well above the l value at which the fission barrier is expected to vanish. Moreover, they find that the width of the mass distribution increases rapidly for l values in excess of the liquid drop limit.

Further evidence that one is not dealing with the fission of a true compound nucleus has come to light in the attempts by Beckermann and Blann (1978) to fit the excitation functions of the 'fusion–fission' component of the reaction Ag+Ar. They have shown that it is not possible to fit the experimental cross sections over a broad energy range without scaling down the liquid drop fission barrier by about 40%. This reduction is apparently necessary to allow fission to compete favourably with the evaporation of neutrons and light charged particles. On the other hand, the 'discrepancy' between data and theory could be avoided without sacrificing the liquid drop fission barrier by assuming that at least some fraction of the 'fission' yield is due to another mechanism which does not have to compete with particle evaporation.

Only recently have theorists tackled the problem of the long-lifetime component. Nörenberg and Riedel (1979) have developed a model in which the interaction times for the mass diffusion process is calculated with a time-dependent ion–ion potential. This potential is a time-dependent mixture of the diabatic and adiabatic potentials. A trajectory calculation is shown in figure 19. Three distinct processes can be identified in the model calculations for the reaction ^{208}Pb+400 MeV ^{40}Ar. For the highest l, the ions scatter inelastically (deep inelastic scattering). For low l, the ions fuse (compound-nucleus formation). For intermediate l, the trajectories become trapped for times comparable to the relaxation time for the mass asymmetry mode ('fusion–fission').

A somewhat different approach has been taken by Mathews and Moretto (1979). In their model they consider the effect of thermal barrier penetration on trajectories which are trapped in the pocket of the ion–ion potential (see figure 8). These trapped systems can live for long times and equilibrate with respect to the mass asymmetry coordinate before they decay. Figure 20 shows the quality of the fit obtained from this model. Clearly both the deep inelastic and fusion–fission components are well reproduced.

Another possible explanation of the mass-equilibrated component is neck formation between the fragments comprising the di-nuclear complex. If a sizeable neck formed during the interaction, the entrance channel asymmetry might quickly be forgotten, leading to a rapid equilibration of the mass asymmetry mode. This line of investigation has recently been pursued by Swiatecki (1979).

5.6. Coupling between mass transfer and energy dissipation

During the collision of two heavy ions the dissipation of kinetic energy and the transfer of mass proceed simultaneously. Consequently, it is clear that there is correlation between these two processes. The coupling between the energy loss and the mass transfer, which

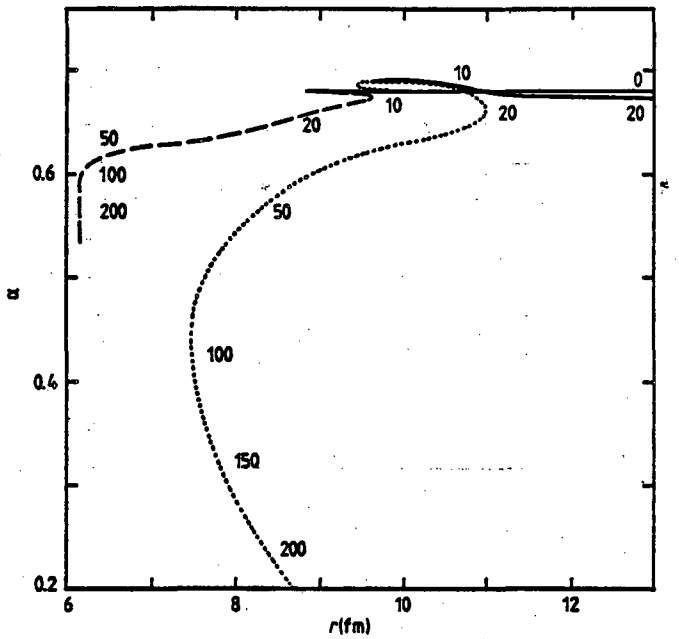

Figure 19. Calculated trajectories for the three l values in the plane defined by the mass asymmetry α ($\alpha=0.5$ corresponds to symmetric decay) and the fragment separation distance r. ——, $b=4.5$ fm, $l=104$; — —, $b=4.4$ fm, $l=102$; · · · · ·, $b=2.2$ fm, $l=0.51$. Values of t are given at various points on the curves in units of 10^{-22} s.

was first emphasised by Huizenga *et al* (1976), is readily observable in a plot of the width of the angle-integrated charge distributions as a function of kinetic energy loss. Such a plot is shown in figure 21 for the reaction $^{209}Bi+^{136}Xe$ (data from Schröder *et al* 1978). At small energy losses the charge distributions consist of a very narrow peak close to the entrance channel asymmetry. At progressively larger energy losses (smaller kinetic energies), one observes a continuous broadening of the Z distributions.

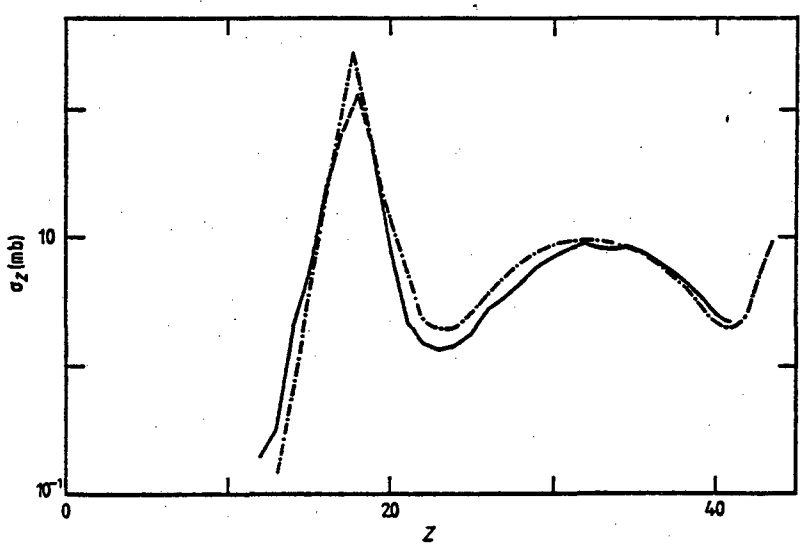

Figure 20. Deep inelastic and fusion–fission components in the reaction 170 MeV $^{40}Ar+^{107,109}Ag$. The full curve represents the data and the broken curve the calculated cross section.

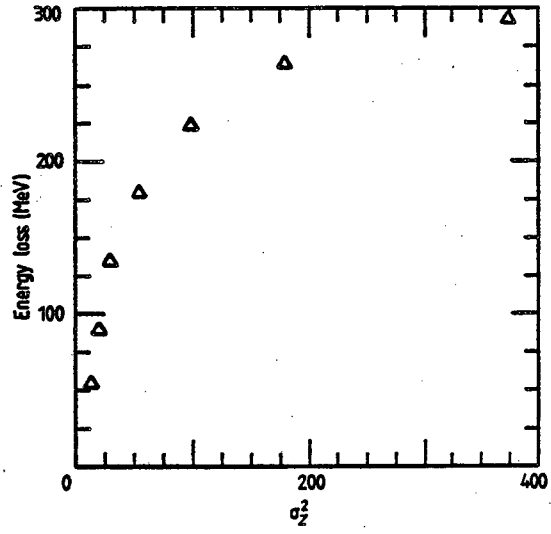

Figure 21. Total energy loss plotted against the variance of the charge distribution for the reaction ^{209}Bi+1130 MeV ^{136}Xe.

At the qualitative level these trends are easy to understand in terms of notions developed earlier. Larger and larger energy losses correspond to longer and longer interaction times. The longer the interaction time, the more extensive the relaxation of the mass asymmetry and hence the broader the Z distributions. As a general observation, it should be pointed out that any of the collective modes excited in deep inelastic collisions can provide us with at least a relative time scale. For example, we have seen that the angular rotation of the fragments is very useful in this regard. Likewise the energy loss also proves to be a useful measure of the interaction time, particularly because it is so easy to determine experimentally.

In order to use the energy loss as an absolute measure of the time scale a calibration procedure has been developed (e.g. Schröder *et al* 1978). The first step involves establishing the relationship between the energy loss and the orbital angular momentum. This is accomplished by dividing the angle and charge-integrated energy spectrum into energy loss bins. The cross section in each of these bins can be associated with an average l value given a knowledge of the total reaction cross section (which defines the number of l waves which contribute) using the relationship

$$\sigma = \pi \lambda\!\!\!^{-2} (l_m + 1)^2$$

where σ is the cross section and $\lambda\!\!\!^{-}$ is the de Broglie wavelength divided by 2π. This procedure is illustrated in figure 22(a).

The absolute interaction times can now be calculated from the experimental average angular deflection, $\delta\theta$, of the fragments in each energy bin via the relation

$$t(l_1) = \delta\theta(l_1)\, \mathscr{I}(l_1)/(\hbar l_t)$$

where $\mathscr{I}$ is the moment of inertia, l_1 is the initial orbital angular momentum and l_t is the final orbital angular momentum. In order to calculate l_t and $\mathscr{I}$ additional assumptions must be made. As limiting cases one can consider non-sticking (no l transfer) and sticking (rigid rotation) of the fragments. The former implies that $l_t = l_1$ and $\mathscr{I} = \mu r^2$ while the latter implies $l_t = l_1\, \mu r^2/\mathscr{I}_s$, where $\mathscr{I}_s$ is the total moment of inertia of the rigid di-nuclear system. In view of γ-ray multiplicity measurements, the first assumption is

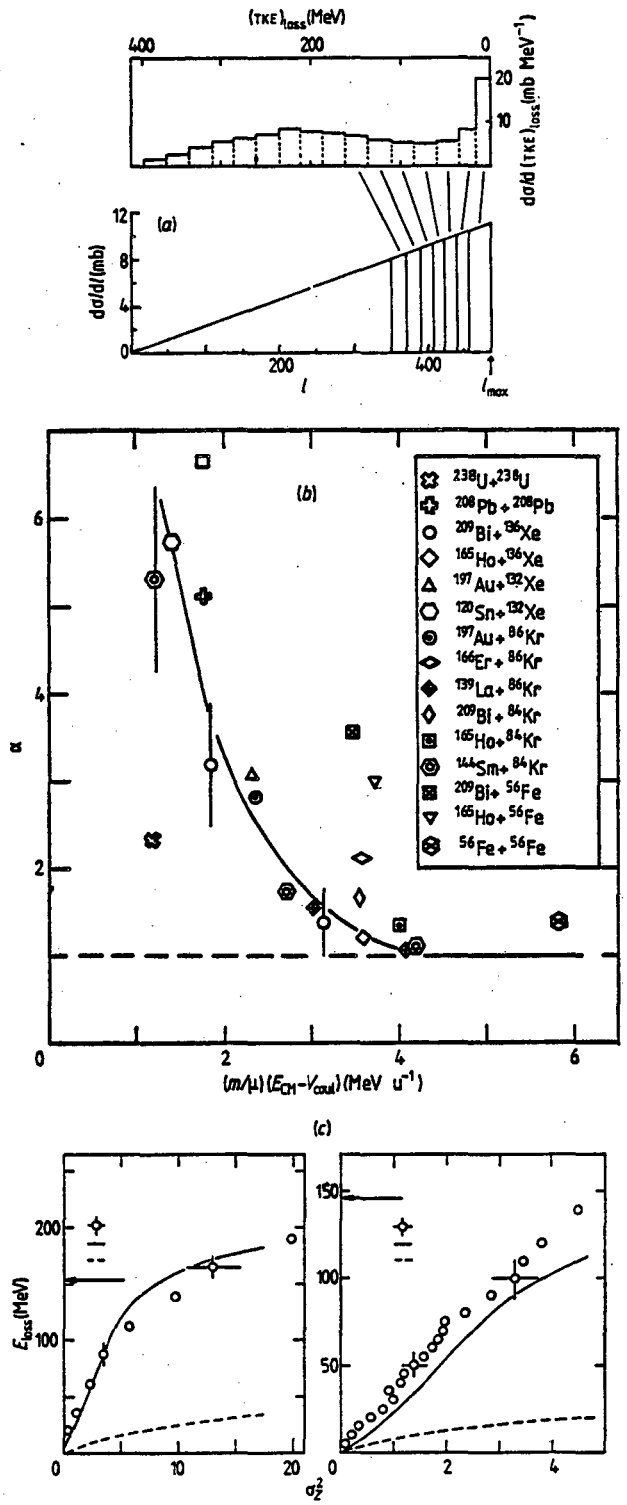

Figure 22. (*a*) Illustration of the procedure to correlate the measured energy loss with the initial angular momentum. The experimental energy loss distribution is shown at the top. The differential cross section $d\sigma/d\Omega$ is plotted against l at the bottom using the sharp cut-off approximation. (*b*) Values of the parameter α obtained from fits to available data plotted against the initially available energy per nucleon above the Coulomb barrier. (*c*) Comparison of model predictions for the correlation $E_{loss}(\sigma z^2)$ with data (○) for the reactions $^{209}Bi+^{136}Xe$ at 940 MeV (left) and $^{209}Bi+^{56}Fe$ at 465 MeV (right). The broken curves represent the classical limits and the full curves are the full calculations.

close to reality in the region of small energy losses whereas the second assumption should be approached for large energy losses (see §7).

Having established a time scale, one can use the experimental charge distributions and solutions to the Fokker–Planck equation to determine transport coefficients. For a linear driving potential the variance of the Z distributions σ_Z^2 is given by

$$\sigma_Z^2 = 2\mu_2 t(l).$$

Diffusion constants extracted using this prescription are comparable to those obtained with other methods. For example, an analysis of the Bi+Xe reaction yields (Schröder *et al* 1978) a mass diffusion constant in the range 0.7×10^{22} s^{-1} (sticking) to 1.1×10^{22} s^{-1} (non-sticking) which are to be compared with a value of 0.5×10^{22} s^{-1} obtained in an analysis of the Au+Kr reaction (Russo *et al* 1977).

If the charge transfer process is truly a random walk problem, the number of exchanged protons is related to the variance of the charge distribution by $N_Z = \sigma_Z^2$. If the exchange of neutrons and protons is correlated, the total number of exchanges N_A is related to σ_Z via

$$N_A \cong (A/Z)^2 \, \sigma_Z^2.$$

In the spirit of a one-body dissipation mechanism the number of exchanged nucleons is related to the energy loss. Hence one can attempt to relate the measured energy loss with the width of the Z distribution using the above equation (Schröder *et al* 1978).

When a nucleon is exchanged between the fragments, its relative momentum $p = mv$ is dissipated, resulting in an energy loss

$$\delta E = (m/\mu) \, E$$

where E is the total available energy ($E = E_{cm} - V_{coul} - E_{loss}$). Predictions based on this equation are compared with experiments in figure 22(*c*). Since the predicted energy loss curves (broken curves) fall well below the experimental data, it would appear that nucleon exchange alone cannot be responsible for the energy dissipation. This observation has led to the suggestion (Randrup 1979, Schröder *et al* 1980) that a substantial number of classically allowed exchanges are blocked because of the Pauli exclusion principle. As a result the energy loss per nucleon exchange is given by

$$\delta E = (m/\mu) \, \alpha E$$

where the parameter α depends on the reaction. Values of α obtained from fits to experimental data are shown in figure 22(*b*) as a function of the available energy per nucleon above the Coulomb barrier. Note that for many reactions α is substantially larger than unity (which corresponds to no Pauli blocking). Calculations including the effect of Pauli blocking are shown in figure 22(*c*) (full curves) for two reactions. The agreement with experiment is vastly improved over the classical calculation.

Despite the agreement with experiment the reader should be cautioned that the above may not represent the final word on the energy dissipation mechanism. The above conclusions depend on the validity of empirical prescriptions which have not yet been fully justified. In fact, the procedure for deducing the angular momentum and hence the time scale from the energy loss spectrum has been challenged (Sventek and Moretto 1978).

6. Isospin fluctuations and giant isovector modes as seen through the isobaric charge distributions

Neutrons and protons are a narrowly split hadron doublet which we call the nucleon. The two components of the doublet are distinguished by a quantum number called isospin, in analogy with spin doublets. The proton has isospin projection $\frac{1}{2}$ and the neutron $-\frac{1}{2}$. The coexistence of both neutrons and protons in nuclear systems implies the coexistence of two very similar but distinct Fermi systems coupled to each other by the nuclear mean field. The exchange component of nucleon–nucleon interaction allows for the transformation of a proton into a neutron through the exchange of a charged virtual π meson. The strong degeneracy of the two Fermi components implies a tendency of nuclei to match their Fermi surfaces. This is realised by equalising the number of neutrons and protons to the extent permitted by the Coulomb energy.

Local disturbances in the neutron-to-proton ratio propagate as a sound wave called isospin sound. In this collective motion the neutrons move out of phase with respect to the protons. The isospin sound has a velocity given by

$$u \cong (Q\chi/m)^{1/2} \cong 0.21c \tag{6.1}$$

where m is the nucleon mass and χ is defined in terms of the potential energy associated with a given fluctuation in neutron-to-proton ratio

$$V = \chi \int \frac{(\rho_n - \rho_z)^2}{\rho_0} \, d\tau$$

where ρ_n, ρ_z and ρ_0 are the neutron, proton and total density, respectively.

Standing waves associated with isospin sound are known as isovector modes. These modes are to be distinguished from the isoscalar modes which involve an in-phase motion of neutrons and protons.

These isovector modes are to be compared to plasmonic excitations observed in other many-body systems, like plasmas and solids where collective fluctuations in charge density can occur. Like plasmons, the isovector modes in nuclei can be excited electromagnetically. By far the best known is the lowest multipole isovector mode called the giant E1 mode. It appears in nuclei as a resonance in the γ-ray absorption cross section at an energy $E \cong 80\, A^{-1/3}$ MeV and with a width of 4–6 MeV. The quadrupole deformation present in certain nuclei splits the resonance into two components. The lower-energy component corresponds to oscillations occurring along the major axis of the football-like nuclear spheroid, while the higher-energy component corresponds to the two degenerate oscillations perpendicular to the elongation axis.

Isovector modes are thought to play a role in the determination of the charge of the fragments at fixed mass asymmetry since the variation of the charge can be produced by out-of-phase movement of neutrons and protons (Brosa and Krappe 1978, Moretto *et al* 1979, 1980, Brosa 1979, Hofmann *et al* 1979). Various observations suggest that the mass asymmetry degree of freedom develops quite slowly in time so that the charge of each of the two fragments adjusts adiabatically, namely at fixed mass asymmetry.

The first moments of the charge distributions at fixed mass asymmetry can be reproduced by requiring that the potential energy of the system at fixed mass asymmetry as a function of charge be at a minimum (Gatty *et al* 1975, Kratz *et al* 1977, Chiang *et al* 1979, Breuer *et al* 1979), or

$$\partial V/\partial Z_1|_{A_1} = 0.$$

More specific information regarding the role of the isovector modes is obtained from the second moment of the charge distribution at fixed mass asymmetry. Since the observed distributions are approximately Gaussian, the fluctuations can be characterised by the standard deviation σ^2 of the distributions.

An immediate, though not necessarily warranted, approximation has been made by assuming that only the lowest isovector multipole (corresponding to the E1 mode, like in the giant dipole resonance) is involved in the isobaric charge fluctuations. If the phonon energy of the dipole mode is $\hbar\omega$ and the stiffness constant is c, then two limiting situations arise. The first corresponds to the case in which the collective mode is weakly coupled to the other modes. In this limit and for $T \ll \hbar\omega$ one would expect only ground-state quantal fluctuations for which

$$\sigma^2 = \hbar\omega/2c.$$

On the other hand, if $T \gg \hbar\omega$ (always weak coupling) or if the collective mode is so strongly coupled to the continuum that its strength function is very spread out, one obtains the classical limit in which the fluctuations depend only upon the temperature T:

$$\sigma^2 = T/c.$$

If, during the decay stage the decoupling from adiabaticity occurs while the neck between the two fragments is still very large and the weak coupling limit holds, one would expect $\hbar\omega \cong 96/d$ MeV where d is the distance between the two fragment centres. In this case $\hbar\omega \gg T$ in most reactions and *large* fluctuations, of the order of $\sigma^2 \cong 1\ e^2$, should be observed, independent of excitation energy. On the other hand, if the strong coupling limit prevails, one would expect fluctuations of perhaps $\sigma^2 \cong 0.3\ e^2$ which increase with excitation energy.

Extraordinarily enough, both situations are observed in various reactions as illustrated in figure 23. It is conceivable that this ambiguity can be resolved by considering the role of the higher-order isovector modes on the one hand, and of the mass asymmetry on the other. This can be shown with the aid of a simple model which points out important facts which have been overlooked (Moretto *et al* 1980).

We shall disregard the extremely important dynamical aspects of the problem and assume that the particular shapes considered in our model just precede the rapid division into two fragments. In particular, let us consider the axial isovector modes in a cylinder of length $2a$, radius r, which is suddenly split at a distance b from one of the bases. The standing isovector waves are trigonometric functions and the boundary conditions require them to be cosine functions.

The fluctuation of the charge density for the mode of order n is

$$\rho_z = -\tfrac{1}{2}\rho_z{}^0 a_n \cos k_n x$$

where $\rho_z{}^0$ is the equilibrium charge density, a_n is the amplitude of the mode, x is the distance along the cylinder axis from one of the bases, and the wavenumber k_n is given by $k_n = (\pi/2a)\, n$. The frequency of each mode is given by $\omega_n = k_n u$, where u is the isospin sound velocity given in equation (6.1)

If we cut the cylinder at b, we can define the charge excess of one of the fragments by the relation:

$$Z_n = -\tfrac{1}{2}\,\rho_z{}^0 a_n\, \pi r^2 \int_0^b \cos k_n x \mathrm{d}x = -\frac{a_n Z}{2\pi}\,\frac{\sin(n\pi Q)}{n}$$

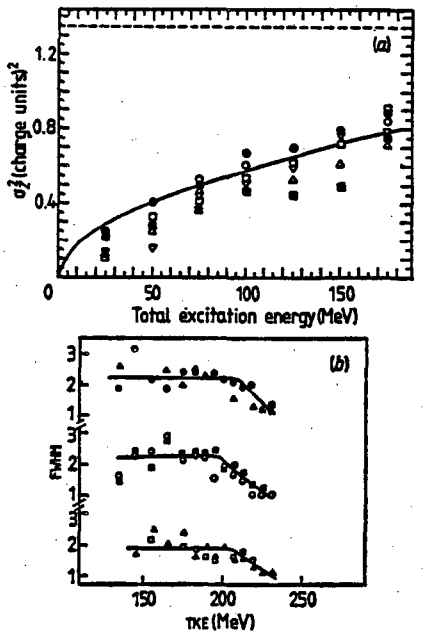

Figure 23. (*a*) Variances of the Z distributions at fixed mass asymmetry plotted against excitation energy in the reaction Xe+Au. The broken and full curves indicate the expected variance from quantal and classical statistical fluctuations (Wirth *et al* 1979). ●, $A=195$; ○, $A=196$; □, $A=197$; ▽, $A=198$; △, $A=199$; ■, $A=200$. ---, $\sigma_Z^2=\hbar\omega/2c$; ——, $\sigma_Z^2=T/c$. (*b*) Widths of the Z distributions for several masses plotted against the total kinetic energy for the reaction ^{86}Kr+^{98}Mo at 430 MeV (Berlanger *et al* 1979). △, $M=87$; ●, $M=88$; ■, $M=86$; ○, $M=85$; ▲, $M=84$; □, $M=83$.

where the degree of symmetry $Q=b/2a$. Since the transformation from the coordinate x to the variable Z_n does not involve time, we can conclude that Z_n oscillates harmonically, because a_n does. Classically, for a fixed value of Q, each Z_n is a separate normal mode. The potential energy is indeed quadratic in Z_n: $V=\frac{1}{2}c_nZ_n^2$ with the stiffness constant c_n given by

$$c_n=\chi\frac{A}{Z^2}\pi^2\frac{n^2}{\sin^2(n\pi Q)}. \tag{6.2}$$

Note that the stiffness constant strongly depends on n. For any n some of the charge fluctuations average out and do not contribute to the fragment charge fluctuation; this is all the more true for large n since it takes more energy to displace a given amount of charge into any given fragment. Even for the lowest mode ($n=1$), some of the energy goes into polarising the fragments rather than displacing charge. This is to be contrasted with the standard way in which c_{LD} has been calculated by using a potential which neglects fragment polarisation. In figure 24, c_1 and c_{LD} can be compared as a function of Q. The large error introduced by neglecting the fragment polarisation is obvious, especially at large asymmetries.

Notice also that for the special values of Q for which $\sin(n\pi Q)$ is zero, the stiffness constant is infinite; no matter how much work is done, no charge displacement arises. This is true in particular at symmetry ($Q=\frac{1}{2}$), where none of the even modes contributes to the charge displacement.

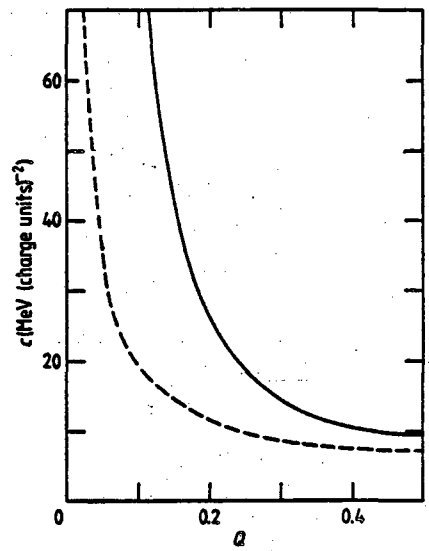

Figure 24. The stiffness constant for the oscillation of the charge excess is plotted against asymmetry for $A=100$. The broken curve corresponds to the liquid drop potential for two touching spheres. The full curve corresponds to the cylinder model for the lowest mode. The contributions of the Coulomb energy have been included for both.

After having identified the Z_n as classical normal modes, we can immediately quantise them. For each mode we obtain a phonon energy

$$\hbar\omega_n = \frac{\hbar u\pi}{2a}\, n.$$

These phonon energies are very large even for the lowest modes, so that the limit $T/\hbar\omega_n \ll 1$ is typically encountered ($T \cong$ nuclear temperature) and only zero-point fluctuations need to be considered.

For each mode n, the zero-point charge width is given by

$$\sigma_n^2 = \frac{\hbar\omega_n}{2c_n} = \sigma_1^2\,(\text{symmetry})\,\frac{\sin^2(n\pi Q)}{n}. \tag{6.3}$$

From figure 25 and equation (6.3), one expects these widths to be smaller at large asymmetries than those calculated neglecting fragment polarisation. The contribution of the nth mode to σ^2 goes like $1/n$, so that the contribution of the higher modes becomes less relevant at higher values of n. However, the total charge width in this model diverges logarithmically:

$$\sigma^2 = \sigma_1^2\,(\text{symmetry})\sum_n \frac{\sin^2(n\pi Q)}{n}. \tag{6.4}$$

This is not surprising because we are assigning an infinite number of degrees of freedom to a system of finite particle number. Furthermore, it is likely that the higher-frequency modes 'drown' in the doorway states directly coupled to them, thus removing the collectiveness from the respective degrees of freedom.

A very important feature of this model is that the role of each mode strongly depends upon the asymmetry of the system. In figure 25(*a*) the normalised partial width is given as a function of asymmetry for a few values of n. In figure 25(*b*), they are given as a

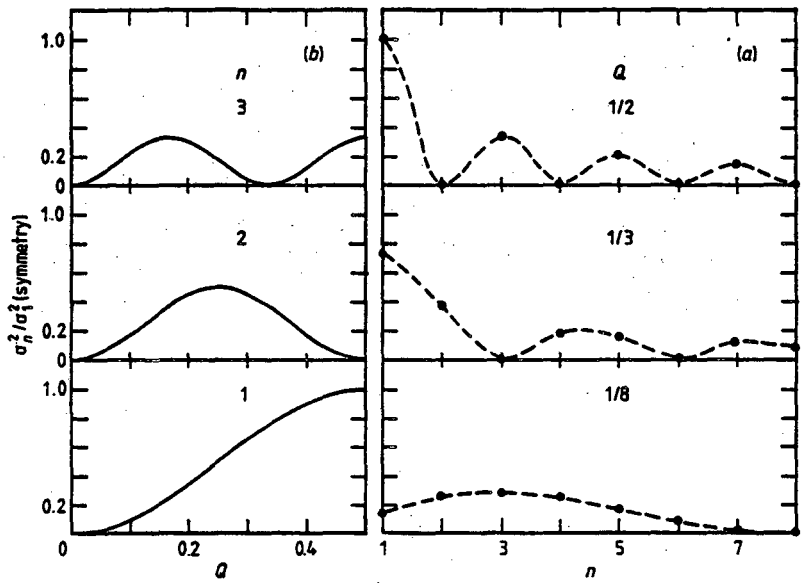

Figure 25. The square of the normalised partial width is plotted (*a*) against the degree of symmetry at fixed n, and (*b*) against n at a fixed asymmetry.

function of n for a few asymmetries. At values close to symmetry, the lowest mode dominates, but with increasing asymmetry the higher n modes play an ever-increasing role. The widths are zero when a half-multiple of the wavelength for a mode matches the value of b. In figure 26 the width arising from the first n modes is given for a few n values as a function of Q. This shows that an experimentally observed width, especially in asymmetric systems, may include the comparable contribution of several modes.

It is clear that any attempt to relate such a width to a single E1 mode rather than to the combination of several isovector modes may be doomed to failure. The difficulties

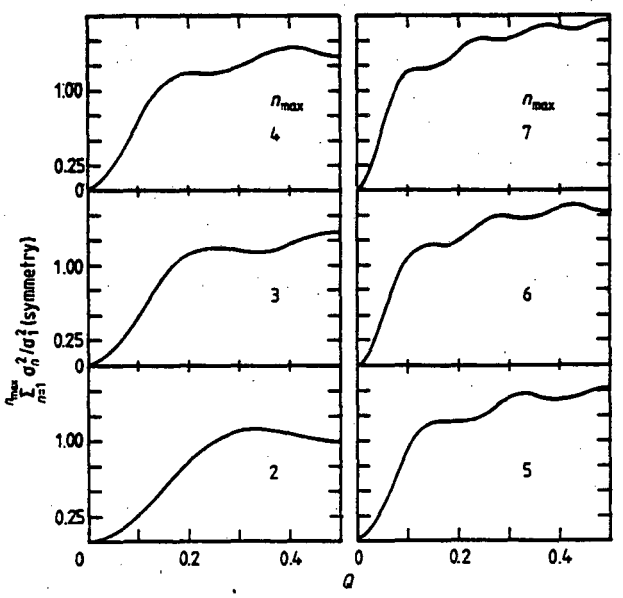

Figure 26. The sum of the squares of the normalised partial width up to n_{max} is plotted against asymmetry.

are compounded by the use of a stiffness constant which may dramatically depend on the form of the standing wave.

In conclusion, information on the isovector modes from the measurement of the charge fluctuation at high temperatures can only be obtained by properly accounting for the effect of mass asymmetry and the role of higher-order modes. Potentially, hidden in the charge distribution and in its dependence upon mass asymmetry and excitation energy lies valuable information on the spreading width of giant isovector modes at high excitation energy which is not accessible by means of conventional techniques like electron scattering or γ-ray absorption.

7. The relaxation of the rotational degrees of freedom

7.1. The equilibrium limit

The relaxation of the rotational degrees of freedom can be best appreciated if one considers two spheres which, during the collision, interact through conservative and dissipative forces. The torques so generated induce a rotation of the fragments. The secular equilibrium, which is eventually attained if the two spheres interact for a sufficiently long time, corresponds to rigid rotation, namely to the regime characterised by the matching of the orbital and intrinsic angular velocities. The angular momentum partition between orbital and intrinsic angular momentum is then fixed, and depends upon the mass ratio of the two fragments:

$$\frac{I_{\rm int}}{I_{\rm tot}}=\frac{\mathcal{I}_1+\mathcal{I}_2}{\mu d^2+\mathcal{I}_1+\mathcal{I}_2}$$

where $I_{\rm int}$, $I_{\rm tot}$ are the intrinsic and total angular momenta, μ is the reduced mass, d is the distance between centres, $\mathcal{I}_1$, $\mathcal{I}_2$ are the momenta of inertia for the two fragments. This ratio is $\frac{2}{7}$ at symmetry (for two touching equal spheres) and increases with increasing mass asymmetry until it reaches 1 for the maximum asymmetry in which one of the two spheres is vanishingly small.

In literature an intermediate limit is often quoted: the 'rolling limit'. This somewhat artificial limit corresponds to the assumption that only 'sliding friction' is acting, until the two touching surfaces do not slide any longer, and no 'rolling friction' is acting on the system. This limit requires the matching of peripheral velocities and, for two touching spheres, predicts an angular momentum ratio:

$$I_{\rm int}/I_{\rm tot}=2/7$$

irrespective of the asymmetry. A lack of practical significance for this limit is expected in the general case in which both 'sliding' and 'rolling friction' are simultaneously active. Under these circumstances the rolling limit is never attained.

The rigid rotation limit is visibly attained in certain reactions where the deep inelastic process is associated with a rather narrow angular momentum window (Ishihara *et al* 1976, Glässel *et al* 1977, Natowitz *et al* 1978). Such a limit is demonstrated by the rising γ-ray multiplicity with increasing mass or charge asymmetry (figure 3).

The techniques commonly used to measure the angular momentum transferred from orbital motion into fragment rotation or spin rely on the sequential emission of particles or γ-rays from the outgoing fragments. Perhaps the easiest technique to understand, if not to apply, is the measurement of the mean γ-ray multiplicities, or the mean number of

γ-rays emitted by the fragments after collision. Other techniques that have been used to measure the fragment angular momentum are based upon the angular distributions of particles (α) emitted by the fragments (Ho *et al* 1977, Babinet *et al* 1980) or the angular distributions of the fragments arising from sequential fission of one of the deep inelastic fragments (Dyer *et al* 1977, Wozniak *et al* 1978, Harrach *et al* 1979, Specht 1979, Glässel *et al* 1979). The principle of these methods is more involved and will be discussed later on. Basically, the larger the fragment spin, the more tightly the sequential fragments are concentrated in the reaction plane. The advantage of this technique is that frequently one can measure the spin of one fragment at a time, rather than the sum of the two fragment spins, as is the case in γ-ray multiplicity measurement.

7.2. The relation between angular momentum transfer and energy dissipation

The correlation between energy dissipation and angular momentum transfer is expected to be quite strong because the dissipative forces associated with energy damping should be well localised and should give rise to strong torques between the two fragments. This effect is abundantly verified experimentally as illustrated, for instance, in figure 27. A

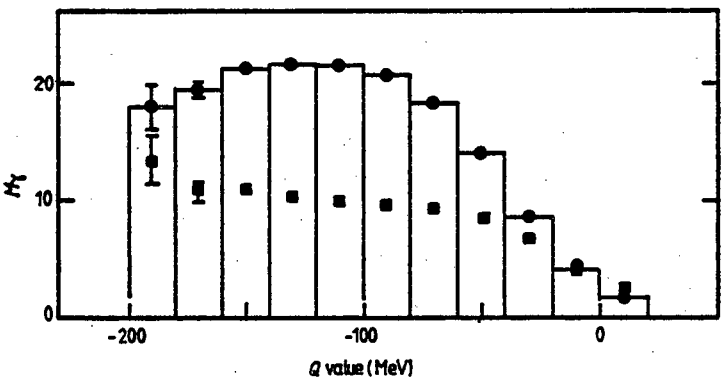

Figure 27. γ-ray multiplicity (●) and sigma (■) of the multiplicity distribution as a function of the Q value for the reaction Sm+Kr (Christensen *et al* 1978) at 43° in the laboratory.

rapid rise of the γ-ray multiplicity with decreasing exit channel kinetic energy is typically observed, followed by a saturation and, at times, by an actual decrease of the γ-ray multiplicity at the very lowest kinetic energies. The rise is, of course, due to the increase in strength and/or duration of the torques, the saturation and the decrease is due to the progressively lower l waves contributing to the low kinetic energy region and also to neutron emission.

Two extreme models for the process of energy dissipation have been proposed, the excitation of giant modes on the one hand and the nucleon transfer on the other. Both of these models predict the large energy losses compatible with experimental observations. There has been some hope that the correlation between energy loss and angular momentum transfer predicted by the two models may be so different that the experimental data could decide in favour of either one, or point to a combination of the two mechanisms.

7.3. Dependence of the γ-ray multiplicity upon mass asymmetry

In the light of the above discussion, a study of the angular momentum transfer as a function of energy and *mass asymmetry* should be more useful, because the varying asymmetry

is certainly associated with net mass transfer, although the total number of nucleon exchanges back and forth may not be easy to determine experimentally.

From the relatively scant experimental evidence, one can summarise the experimental situation as follows: (*a*) in the quasi-elastic region, the dependence of the γ-ray multiplicity upon mass asymmetry is V-shaped, with the minimum at the entrance channel asymmetry (figure 28(B, D)); (*b*) in the deep inelastic region, the γ-ray multiplicity increases with increasing asymmetry when the deep inelastic process involves a narrow l window (figure 3) but usually stays more or less constant with mass asymmetry (Berlanger *et al* 1976, Aleonard *et al* 1978, Christensen *et al* 1978, Olmi *et al* 1978) when the deep inelastic process involves a very large l window (figure 28(A, C)).

The V-shaped dependence of the γ-ray multiplicity in the quasi-elastic region can be explained either in terms of the angular momentum transfer associated with mass transfer

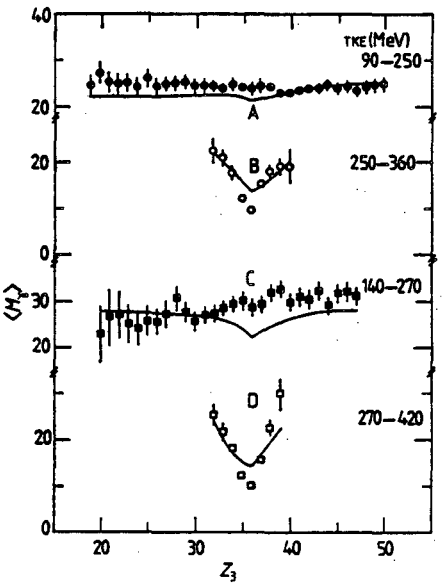

Figure 28. γ-ray multiplicities as a function of Z for the reactions Kr + Ag (curves A and B) and Kr + Ho (curves C and D) (Regimbart *et al* 1978). The full symbols represent deep inelastic reactions while the open symbols represent quasi-elastic reactions. The full curves are fits to the data.

or (and it may be the same thing) by the fact that the average energy loss increases as one moves away from the entrance channel asymmetry.

The rising γ-ray multiplicity with increasing asymmetry for narrow l windows may be directly attributed to rigid rotation. On the other hand, the flat dependence of the γ-ray multiplicity against mass asymmetry for broad l windows does not necessarily imply the absence of rigid rotation. Rather it is most likely due to angular momentum fractionation along the mass asymmetry coordinate. The experiments suggest that the interaction times are a decreasing function of angular momentum. Furthermore the spreading of the cross section along the mass asymmetry appears to increase with increasing interaction times. As a consequence the high l waves populate configurations with asymmetries close to the injection asymmetry, while the low l waves can spread further out to much greater asymmetries. Thus the average entrance channel angular momentum should decrease as one moves away from the entrance channel asymmetry. In particular, the decrease in the average l wave as one moves towards larger asymmetries (lower Z)

may compensate for the rising trend required by the rigid rotation condition, leading to a very weak dependence of the fragment spin (and hence the γ-ray multiplicity) upon mass asymmetry (Regimbart *et al* 1978, Wolschin and Nörenberg 1978a, b, Gerschel *et al* 1979, Moretto and Schmitt 1980). Additional evidence supporting this angular momentum fractionation along the mass asymmetry coordinate has been obtained in studies of the variation of the mean energy of the relaxed peak with exit channel asymmetry (Simbel and Adul-Magd 1980, Adler *et al* 1980).

7.4. Alignment and polarisation of the fragment angular momentum

The torques associated with the frictional forces acting between target and projectile during their interaction should induce a spin in the fragments which is aligned with the total angular momentum, and perpendicular to the reaction plane. This alignment and polarisation can be used to determine whether the fragments are scattered at positive or negative angles by measuring, for instance, the circular polarisation of the γ-rays emitted by the fragments. Clear-cut cases of positive scattering angles have been demonstrated for the strongly focused reaction 612 MeV ^{86}Kr+^{197}Au through the substantial negative circular polarisation of the emitted γ-rays. Cases of weak polarisation have been observed in the reaction Kr+Ag and have been interpreted in terms of contributions to the cross section from opposite sides of the interaction region (Trautmann *et al* 1977, Lauterbach *et al* 1978).

Angular momentum misalignment occurs when in-plane components of the angular momentum are present. These components can be generated either directly by some feature of the reaction mechanism (Ayik *et al* 1978, Zielinska-Pfabe 1978, Vandenbosch 1979) or can be associated with thermal fluctuations of the angular-momentum-bearing modes (Wozniak *et al* 1978, Moretto and Schmitt 1980). The angular momentum misalignment can be determined by measuring the angular distributions of particles or photons emitted by one or both fragments, or of sequential fission fragments. Measurements of the sequential fission fragment angular distributions (Dyer *et al* 1977, Wozniak *et al* 1978, Harrach *et al* 1979) as well as of α-particles (Ho *et al* 1977, Babinet *et al* 1980) and γ-rays (Van Bibber *et al* 1977, Berlanger *et al* 1976, Dayras *et al* 1979, Aguer *et al* 1979, Wozniak *et al* 1980, Puigh *et al* 1980) have been performed. The analysis of these data requires expressions for the in- and out-of-plane angular distribution, and their specific dependence upon the distributions of the three angular momentum components. We shall use the assumption that the angular momentum misalignment actually arises from equilibrium statistical fluctuations. This assumption has been verified in a variety of experiments, as we shall see later on.

7.5. Statistical excitation of angular-momentum-bearing modes

Let us consider a frame of reference where the z axis is parallel to the entrance channel angular momentum, the x axis is parallel to the recoil direction of one of the fragments, and the y axis is perpendicular to the z, x plane. A misalignment of the fragment angular momentum arises when non-vanishing x and y components of the fragment angular momentum are present. Among the possible sources of these components, the thermal excitation of angular-momentum-bearing modes of the intermediate complex appears very likely and can be readily investigated. Such modes are excited in fission (Wilhelmy *et al* 1972).

If the intermediate complex is assumed to have the shape of two equal touching

spheres, the angular-momentum-bearing normal modes are easily identifiable. In figure 29 these modes are illustrated. We shall call them 'bending' B (doubly degenerate), 'twisting' Tw (degenerate with bending), 'wriggling' W (double degenerate) and 'tilting' Ti. In a recent work, the statistical-mechanical aspects of the excitation of these modes has been studied in detail (Moretto and Schmitt 1980). Here we report only the relevant conclusions.

The thermal excitation of these collective modes leads to Gaussian distributions in the three components I_x, I_y, I_z, namely:

$$P(I) \propto \exp - \left(\frac{I_x^2}{2\sigma_x^2} + \frac{I_y^2}{2\sigma_y^2} + \frac{(I_z - \bar{I}_z)^2}{2\sigma_z^2} \right) \tag{7.1}$$

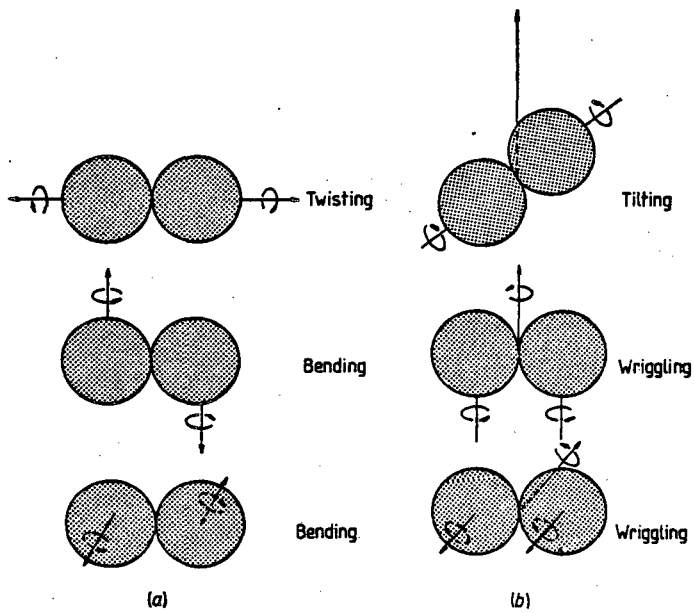

Figure 29. (*a*) Schematic illustrating the twisting mode and the doubly-degenerate bending modes for a two equal spheres model. In each case the spin vectors of the fragments (symbolised by arrows) are of equal length but point in opposite directions. (*b*) Schematic illustrating the tilting mode and the doubly-degenerate wriggling modes for the equal spheres model. The short arrows represent the spin vectors of the fragments. The long arrows originating at the point of tangency of the two spheres represent the orbital angular momentum vectors (see Moretto and Schmitt 1980).

where

$$\sigma_x^2 = \sigma_{\mathrm{Tw}}^2 + \sigma_{\mathrm{Ti}}^2 = \tfrac{1}{2}\mathcal{I}T + \tfrac{7}{10}\mathcal{I}T = \tfrac{6}{5}\mathcal{I}T$$
$$\sigma_y^2 = \sigma_{\mathrm{B}}^2 + \sigma_{\mathrm{W}}^2 = \tfrac{1}{2}\mathcal{I}T + \tfrac{5}{14}\mathcal{I}T = \tfrac{6}{7}\mathcal{I}T$$
$$\sigma_z^2 = \sigma_{\mathrm{B}}^2 + \sigma_{\mathrm{W}}^2 = \tfrac{1}{2}\mathcal{I}T + \tfrac{5}{14}\mathcal{I}T = \tfrac{6}{7}\mathcal{I}T.$$

The quantity $\mathcal{I}$ is the moment of inertia of one of the two touching spheres, and T is the temperature. The assumption of two equal touching spheres is admittedly schematic. However, the generalisation to two equal touching spheroids is completely trivial.

7.6. Angular distributions associated with sequential fission and sequential light particle emission

The magnitude of the angular momentum misalignment can be measured through the

in- and out-of-plane angular distribution of the decay products of one of the two fragments (e.g. Back and Bjørnholm 1978). Examples of the sequential fission fragment angular distributions can be seen in figure 30.

The angular distribution of fission fragments and light particles emitted by a compound nucleus can be treated within a single framework. The direction of emission of a decay product (fission fragment, α-particle, etc) is defined by the projection K of the fragment angular momentum on the disintegration axis. Simple statistical-mechanical considerations show that the distribution in K values is Gaussian:

$$P(x) \propto \exp(-K^2/2K_0^2)$$

where $K_0^2 = \hbar^{-2}(1/\mathcal{I}_\parallel - 1/\mathcal{I}_\perp)^{-1}T$; $\mathcal{I}_\parallel$, $\mathcal{I}_\perp$ are the principal moments of inertia of the

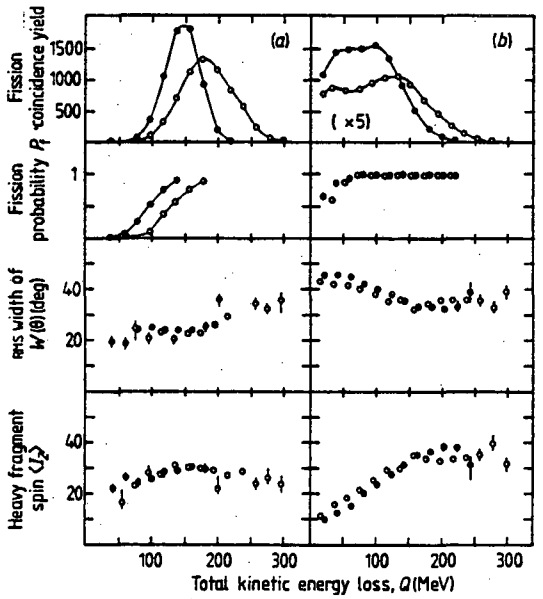

Figure 30. Fission coincidence yield, fission probabilities (ratio of ternaries to total), RMS angles of the polar distributions and a lower limit for the average oriented part $\langle I_z \rangle$ of the heavy-fragment spin assuming complete alignment (from Harrach *et al* 1979). (*a*) ^{208}Pb, (*b*) ^{238}U. ●, ^{58}Ni, ▲, ^{90}Zr.

decaying system with particle and residual nucleus just in contact about axes parallel and perpendicular to the disintegration axis, respectively.

Let us now express the particle decay probability in terms of the emission angle α measured with respect to the angular momentum direction. Since $K = I\cos\alpha$ and $\mathrm{d}K = I\,\mathrm{d}(\cos\alpha) = I\,\mathrm{d}\Omega$, we obtain for the decay width:

$$\Gamma^I(\alpha)\,\mathrm{d}\Omega \propto \exp\left(-\frac{I^2\cos^2\alpha}{2K_0^2}\right)\mathrm{d}\Omega.$$

If the angular momentum has an arbitrary orientation with respect to our chosen frame of reference, defined by its components I_x, I_y, I_z, the angular distribution can be easily rewritten by noticing that

$$K = I\cos\alpha = \boldsymbol{I}\cdot\boldsymbol{n} = I_x\sin\theta\cos\varphi + I_y\sin\theta\sin\varphi + I_z\cos\theta$$

where $\boldsymbol{n}$ is a unit vector pointing in the direction of particle emission with polar angles

θ, φ. If the orientation of the angular momentum is given by the distribution expressed by equation (7.1) we can integrate over the distribution of orientations and obtain, dropping angular-momentum-independent factors (Broglia *et al* 1979),

$$\Gamma^I(\theta, \varphi)\, d\Omega \propto \exp\left[\frac{\hbar^2 I^2}{2T}\left(\frac{1}{\mathscr{I}_\perp}-\frac{1}{\mathscr{I}_c}\right)\frac{1}{S(\theta,\varphi)}\right]\exp\left(-\frac{I^2\cos^2\theta}{2S^2(\theta,\varphi)}\right)d\Omega$$

where

$$S^2(\theta,\varphi)=K_0^2+(\sigma_x^2\cos^2\varphi+\sigma_y^2\sin^2\varphi)\sin^2\theta+\sigma_z^2\cos^2\theta$$

and $\mathscr{I}_c$ is the moment of inertia of the compound nucleus.

The final angular distribution is obtained by integration over the fragment angular momentum distribution which we assume reflects the entrance channel angular momentum distribution through the rigid rotation condition:

$$\frac{d\sigma}{d\Omega}\propto\int_0^{I_{mx}} 2I\, dI\,\frac{\Gamma^I}{\Gamma_N}$$

where we have assumed $\Gamma_T \cong \Gamma_N$. More precisely:

$$W(\theta,\varphi)=\frac{1}{SA}\left[1-\exp(-A)\right]$$

where

$$A=I_{mx}^2\left(\frac{\cos^2\theta}{2S^2}-\beta\right)$$

$$\beta=\frac{\hbar^2}{2T}\left(\frac{1}{\mathscr{I}_n}-\frac{1}{\mathscr{I}_\perp}\right).$$

The quantity $\mathscr{I}_n$ is the moment of inertia of the nucleus after neutron emission, and $\mathscr{I}_\perp$ is the perpendicular moment of inertia of the critical shape for the decay (e.g. saddle point). It is important to notice that the angular momentum dependence of the particle/neutron competition or fission/neutron competition is explicitly taken into account through β.

The final ingredient necessary for an explicit calculation of the angular distributions is the quantity K_0^2. This quantity can be expressed in terms of the principal moments of inertia of the critical configuration for the decay:

$$K_0^2=\frac{1}{\hbar^2}\left(\frac{1}{\mathscr{I}_t}-\frac{1}{\mathscr{I}_\perp}\right)^{-1}T=\mathscr{I}_{eff}T/\hbar^2.$$

For fission $\mathscr{I}_{eff}$ can be taken from the liquid drop calculations. For light particle emission, the calculation of $\mathscr{I}_{eff}$ can be worked out rather easily. Now we are in the position to calculate both in-plane and out-of-plane anisotropies.

The in-plane anisotropy gives

$$\left.\frac{W(\varphi=90°)}{W(\varphi=0°)}\right|_{\theta=90°}=\left(\frac{K_0^2+\sigma_x^2}{K_0^2+\sigma_y^2}\right)^{1/2}.$$

Since in most cases K_0^2 is fairly large, or at least comparable with σ_x^2 or σ_y^2, it is difficult to obtain a sizeable in-plane anisotropy. Even by letting $\sigma_x=0$ one needs $\sigma_y^2=3\,K_0^2$ just to obtain the anisotropy of 2! The out-of-plane anisotropy is somewhat more complicated:

$$\left.\frac{W(\theta=90°)}{W(\theta=0°)}\right|_{\varphi=0°}=\frac{1}{\beta}\left(\frac{K_0^2+\sigma_z^2}{K_0^2+\sigma_x^2}\right)^{1/2}\left(\beta-\frac{1}{2(K_0^2+\sigma_z^2)}\right)\frac{1-\exp(\beta I_{max}^2)}{1-\exp\left(I_{mx}^2\{\beta-[2(K_0^2+\sigma_z^2)]^{-1}\}\right)}.$$

At $\varphi=90°$ the anisotropy is obtained from the above equation by interchanging σ_x with σ_y.

The results obtained above can be illustrated by applying them to a reaction which has been experimentally investigated. We chose the reaction 600 MeV ^{86}Kr+Au (Wozniak *et al* 1978). For this reaction we estimate $\mathcal{I}_{sph}/\mathcal{I}_{eff}=1.864$, $K_0^2=100\,\hbar^2$, $\beta=0.00194\,\hbar^{-2}$, $I_{mx}=40\,\hbar$, $\sigma^2\simeq 110\,\hbar^2$. The result of the calculation are shown in figure 31. The predicted FWHM = 54° is in good agreement with the measured value of ~50°.

In the same spirit as for sequential fission one can investigate the angular distributions of protons and α-particles emitted sequentially. The formalism to be used is essentially identical with the one illustrated above and the results are also in good agreement with the data.

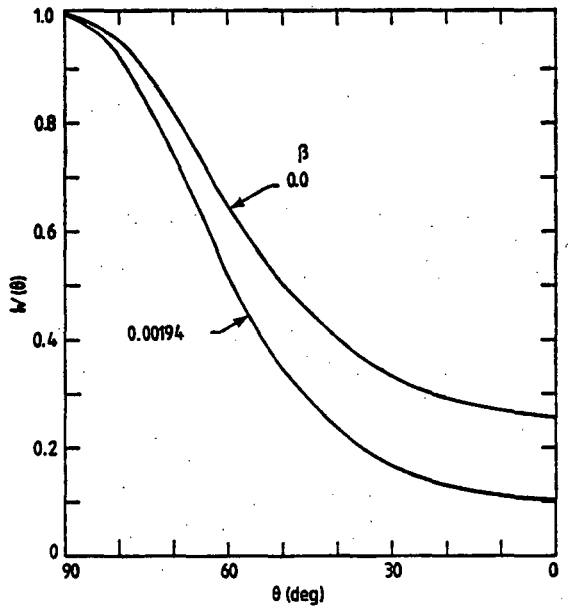

Figure 31. Sequential fission angular distributions calculated for the system 600 MeV Kr+Au. The curve labelled $\beta=0.0$ corresponds to disregarding neutron emission/fission competition. The more realistic curve labelled $\beta=0.001\,94$ gives a FWHM of 54°.

7.7. γ-ray angular distributions and anisotropy experiments

Fragments with large amounts of angular momentum are expected to dispose of it mainly by stretched E2 decay. The relative amounts of dipole and quadrupole radiation depends mainly upon the ability of the nucleus to remain a good rotor over the whole angular momentum range. If the angular momentum of the fragment is aligned, the typical angular pattern of the quadrupole radiation should be observed. Any misalignment should decrease the sharpness of the angular distribution.

For a perfectly aligned system we have (see De Groot and Tolhoek 1955):

$$W(\alpha)=\tfrac{3}{4}(1+\cos^2\alpha) \quad \text{for E1} \qquad W(\alpha)=\tfrac{5}{4}(1-\cos^4\alpha). \quad \text{for E2}$$

If the angular momentum is not aligned with the z axis, one must express α in terms of

θ, φ which define the direction of the angular momentum vector. In particular we have

$$\cos\alpha=\frac{\boldsymbol{I}\cdot\boldsymbol{n}}{I}=\frac{I_x\sin\theta\cos\varphi+I_y\sin\theta\sin\varphi+I_z\cos\theta}{(I_x^2+I_y^2+I_z^2)^{1/2}}.$$

For any given I, the angular distribution is obtained by integration over the statistical distribution $P(I)$ of the angular momentum components:

$$W(\theta,\varphi)=\int W(\alpha)P(I)\,\mathrm{d}I.$$

It is not possible to obtain general analytical expressions. However, if we are willing to assume $\sigma_x^2=\sigma_y^2=\sigma_z^2=\sigma$ then an exact result can be obtained.

For the E1 distribution one obtains

$$W(\theta)_{\mathrm{E1}}=\tfrac{3}{4}[1+\cos^2\theta+\beta^2(1-D(\beta))\,(1-3\cos^2\theta)].$$

For the E2 distribution one obtains

$$W(\theta)_{\mathrm{E2}}=\tfrac{5}{4}\{1-\cos^4\theta-2\beta^2[3\sin^2\theta\cos^2\theta-2\cos^4\theta-\tfrac{3}{4}D(\beta)\,(\sin^2\theta-4\cos^2\theta)\sin^2\theta]$$
$$-3\beta^4[4\cos^4\theta+\tfrac{3}{2}\sin^4\theta-12\sin^2\theta\cos^2\theta\,(1-D)]\}.$$

In these equations $\beta=\sigma/I_z$ and $D(\beta)=\sqrt{2}\beta F(1/\sqrt{2}\beta)$ where

$$F(x)=\exp(-x^2)\int_0^x\exp(t^2)\,\mathrm{d}t$$

is Dawson's integral. One can easily verify that the anisotropy $W(\theta)/W(90°)$ tends to 1 when β tends to infinity both for E1 and E2 transitions, while it tends to 0 for E2 and to 2 for E1 when $\beta=0$. If one has a fairly good experimental idea of the amount of E1 radiation to be expected from a given fragment and of its degree of stretching, the measurement of the anistropy yields directly the value of $\beta=\sigma/I_z$, which is a direct measure of the angular momentum alignment.

The predictions of the model just described can be compared with measured γ-ray anisotropies. Very interesting results have been obtained (Wozniak *et al* 1980) for the system ^{165}Ho+1400 MeV ^{165}Ho. In this experiment the most probable exit channel is symmetric and is in a mass region where a good rotational behaviour is well established. The γ-ray anisotropy has been measured for a set of Q values together with the γ-ray multiplicity. For each Q value bin, the angular momentum can be determined from the γ-ray multiplicity, while the temperature and the neutron emission effect can be estimated from the Q value. The model described above is used to calculate σ^2 for all the Q value bins and the corresponding value of σ^2/I_z^2 is used to calculate the anisotropy. In figure 32 the experimental γ-ray anisotropies are shown as a function of Q value bins. The calculated anisotropy is also shown and it appears to reproduce the experimental data quite well. Qualitatively the dependence of the anisotropy upon Q value can be simply understood. At lower Q values the rate of angular momentum transfer is high and the excitation of the angular-momentum-bearing modes is small. Thus the alignment is quite high, giving rise to a large anisotropy. As the Q value increases, the angular momentum transfer stops, while the thermal excitation of the angular-momentum-bearing modes continues. The angular momentum becomes progressively more misaligned and the anisotropy rapidly decreases.

This field is still too active and much work is still needed to reach definitive conclusions on the subject. However, it is clear that angular momentum fluctuations exist and that they have a characteristic Q value dependence. In particular it is surprising to

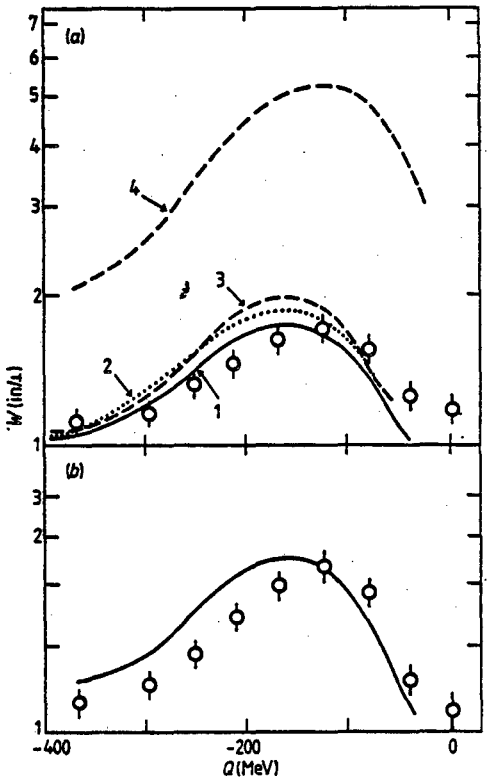

Figure 32. Experimental (symbols) and calculated (curves) values of the anisotropy $W(\text{in}/\perp)$ (*a*) for γ-rays with $E_\gamma > 0.3$ MeV and (*b*) for γ-rays with 0.6 MeV $< E_\gamma <$ 1.2 MeV. The full curves include the effect of neutron emission, E1 transitions and thermal excitation of collective modes. Curve 2 excludes the effect of neutron emission, curve 3 excludes the statistical transitions, and curve 4 excludes the excitation of collective modes.

see how well the predictions of the model based upon the statistical equilibrium treatment of angular-momentum-bearing modes are verified experimentally.

8. Conclusions

The present review had among its various goals that of presenting the rich and varied phenomenology that has become available with the exploitation of the field of heavy ions. These new processes are partly understood in terms of empirical microscopic models, so that a comprehensive qualitative or semi-quantitative grasp of the whole field is now at hand. In this sense, the exploration of the macroscopic variables first considered with the discovery of fission has been successfully expanded and understood in terms of a more or less coherent picture. However, the long-range hope and goal is the understanding of large-scale collective motion of nuclear systems in terms of microscopic variables. This has already been attempted at various levels. One-body dissipation and mass diffusion can be seen to arise as the generalisation of the shell model from static to dynamic systems. A similar progress has been made by introducing time dependence in the self-consistent approach of the time-dependent Hartree–Fock formalism. The inclusion of collision terms may possibly improve TDHF to the point of enabling it to make quantitative predictions for a good fraction of these phenomena. Similarly, the

microscopic understanding of the giant resonances may show their specific role in the processes of both energy dissipation and angular momentum transfer. It is not clear to us as yet how all these partial attempts will merge into a unified and coherent theory. It is clear, however, that the field of heavy-ion reactions has enormously extended the scope and richness of nuclear physics not only by introducing new exciting degrees of freedom, but by making accessible their time evolution.

The great versatility and richness of nuclear systems proves once more the relevance of nuclear physics among the great variety of physical disciplines. There is little doubt that the nucleus is still the most important of the many-body systems and the best challenge so far to our understanding of the many-body problem.

References

Adler L, Gonthier P, Ho JHK, Khodai A, Namboodiri MN, Natowitz JB and Simon S 1980 *Phys. Rev. Lett.* **45** 696

Agarwal S, Galin J, Gatty B, Guerreau D, Lefort M, Tarrago X, Babinet R, Cauvin B, Girard J and Nifenecker H 1977 *Nucl. Phys.* A **293** 230

Aguer P *et al* 1979 *Phys. Rev. Lett* **43** 1778

Albrecht R, Dünnweber W, Graw G, Ho H, Steadman SG and Wurm JP 1975 *Phys. Rev. Lett.* **34** 1400–3

Albrecht K and Stocker W 1977 *Nucl. Phys.* A **278** 95–108

Aleonard MM, Wozniak GJ, Glässel P, Deleplanque MA, Diamond RM, Moretto LG, Schmitt RP and Stephens FS 1978 *Phys. Rev. Lett.* **40** 622

Artukh AG, Gridnev GF, Mikheev VL, Volkov VV and Wilczynski J 1973 *Nucl. Phys.* A **215** 91

Ayik S, Wolschin G and Nörenberg W 1978 *Z. Phys.* A **286** 271–9

Babinet R, Cauvin B, Girard J, Alexander JM, Chiang TH, Galin J, Gatty B, Guerreau D and Tarrago X 1980 *Z. Phys.* A **295** 153–67

Babinet R, Cauvin B, Girard J, Nifenecker H, Gatty G, Guerreau D, Lefort M and Tarrago X 1978 *Nucl. Phys.* A **296** 160

Babinet R, Moretto LG, Galin J, Jared R, Moulton J and Thompson SG 1976 *Nucl. Phys.* A **258** 172

Back BB and Bjørnholm S 1978 *Nucl. Phys.* A **302** 343–64

Beckerman M and Blann M 1977 *Phys. Rev. Lett.* **38** 279

Berlanger M *et al* 1976 *J. Physique Lett.* **37** L323

Berlanger M, Gobbi A, Hanappe F, Lynen U, Ngo C, Olmi A, Sann H, Steltzer HH, Richel H and Rivet MF 1979 *Z. Phys.* A **291** 133

Berlanger M, Ngô C, Grange P, Richert J and Hofmann H 1978 *Z. Phys.* A **284** 61–4

Bethe H 1938 *Phys. Rev.* **53** 675

Bhowmik BK, Pollacco EC, Sanderson NE, England JBA and Morrison G 1978 *Phys. Lett.* **80B** 41

Birkelund J, Tubbs LE, Huizenga JR, De JN and Sperber D 1979 *Phys. Rep.* **56** 107

Blocki J, Boneh Y, Nix JR, Randrup J, Robel M, Sierk AJ and Swiatecki WJ 1978 *Ann. Phys., NY* **113** 330–86

Blocki J, Randrup J, Swiatecki WJ and Tsang CF 1977 *Ann. Phys., NY* **105** 427

Bondorf JP, De JN, Fai G, Karvinen AOT, Jakobsson B and Randrup J 1980 *Nucl. Phys.* A **333** 285–301

Bondorf JP, Sobel MI and Sperber D 1974 *Phys. Lett.* **15C** 83–111

Breuer H *et al* 1979 *Phys. Rev. Lett.* **43** 191–4

Britt HC, Erkkila BH, Stokes RH, Gutbrod HH, Plasil F, Ferguson RL and Blann M 1976 *Phys. Rev.* C **13** 1483

Broglia RA, Dasso CM and Winther A 1974 *Phys. Lett.* **53B** 301

—— 1976 *Phys. Lett.* **61B** 113

Broglia RA, Pollarolo G, Dasso CH and Dössing T 1979 *Phys. Rev. Lett.* **43** 1649–51

Brosa U 1979 *Z. Phys.* A **292** 385–8

Brosa U and Krappe HJ 1978 *Z. Phys.* A **284** 65–9

Businaro VL and Gallone S 1955 *Nuovo Cim.* 1 1102

Cauvin B, Jared RC, Russo P, Schmitt RP, Babinet R and Moretto LG 1978 *Nucl. Phys.* A **301** 511

Chiang TH, Guerreau D, Aguer P, Galin J, Gatty B, Tarrago X and Girard J 1979 *Phys. Rev.* C **20** 1408–18
Christensen PR *et al* 1978 *Phys. Rev. Lett.* **40** 1245–8
Cohen S, Plasil F and Swiatecki WJ 1974 *Ann. Phys., NY* **82** 557
Cusson RY, Maruhn JA and Stocker H 1980 *Z. Phys.* A **294** 257–60
Davies KTR, Sandhya Devi KR and Strayer MR 1979 *Phys. Rev.* C **20** 1372–81
Dayras RA *et al* 1979 *Phys. Rev. Lett.* **42** 697–700
De Groot SR and Tolhoek HA 1955 *Beta- and Gamma-Ray Spectroscopy* ed K Siegbahn (Amsterdam: North-Holland) p 616
Deubler HH and Dietrich K 1975 *Phys. Lett.* **56B** 241–4
Dyer P, Puigh RJ, Vandenbosch R, Thomas TD and Zisman MS 1977 *Phys. Rev. Lett.* **39** 391–5
Ericson T 1960 *Adv. Phys.* **9** 423
Eyal Y *et al* 1978 *Phys. Rev. Lett.* **41** 625–8
Fleury A and Alexander JM 1974 *Ann. Rev. Nucl. Sci.* **24** 279–339
Frascaria N *et al* 1980 *Z. Phys.* A **294** 167–72
Frascaria N, Stephan C, Colombani P, Garron JP, Jacmart JC, Riou M and Tassan-Got L 1977 *Phys. Rev. Lett.* **39** 918–21
Galin J 1976 *J. Physique* **37** C5–83
Galin J, Gatty B, Guerreau D, Lefort M, Tarrago X, Babinet R, Cauvin B, Girard J and Nifenecker H 1976 *Z. Phys.* A **278** 347–52
Galin J, Guerreau D, Lefort M, Peter J, Tarrago X and Basile R 1970 *Nucl. Phys.* A **159** 461
Gamp A, Jacmart JC, Poffe N, Doubre H, Roynette JC and Wilczynski J 1978 *Phys. Lett.* **74B** 215
Gatty B, Guerreau D, Lefort M, Tarrago X, Galin J, Cauvin B, Girard J and Nifenecker H 1975 *Nucl. Phys.* A **253** 511
Gelbke C, Bini M, Olmer C, Hendrie DL, Laville JL, Mahoney J, Mermaz MC, Scott DK and Weiman HH 1977 *Phys. Lett.* **71B** 83
Gelbke CK, Braun-Munzinger P, Barrette J, Zeidman B, LeVine MJ, Gamp A, Harney HL and Walcher Th 1976 *Nucl. Phys.* A **269** 460
Gerschel C *et al* 1979 *Nucl. Phys.* A **317** 473–94
Glässel P, Harrach Dv, Civelekoglu Y, Manner R, Specht HJ and Wilhelmy JB 1979 *Phys. Rev. Lett.* **43** 1483–6
Glässel P, Simon RS, Diamond RM, Jared RC, Lee IY, Moretto GL, Newton JO, Schmitt R and Stephens FS 1977 *Phys. Rev. Lett.* **38** 331–4
Gottschalk PA and Weström M 1977 *Phys. Rev. Lett.* **39** 1250
Gould CR, Bass R, Czarnecki Jv, Hartmann V, Stelzer K, Zitzmann R and Eyal Y 1980 *Z. Phys.* A **294** 323–30
Gross DHE and Kalinowski H 1978 *Phys. Rep.* **45** 175–210
Hanappe F, Lefort M, Ngô C, Peter J and Tamain B 1974 *Phys. Rev. Lett.* **32** 738
Harrach Dv, Glässel P, Civelekoglu Y, Manner R and Specht HJ 1979 *Phys. Rev. Lett.* **42** 1728–32
Harris JW, Cormier TM, Geesaman DF, Lee LL Jr, McGrath RL and Wurm JP 1977 *Phys. Rev. Lett.* **38** 1460
Heusch B, Volant C, Freiesleben H, Chestnut RP, Hildebrand KD, Pühlhofer F, Schneider WFW, Kohlmeyer B and Pfeffer W 1978 *Z. Phys.* A **288** 391
Hilscher D, Birkelund JR, Hoover AD, Schröder WU, Wilcke WW, Huizenga JR, Mignerey A, Wolf KL, Breuer HF and Viola vE Jr 1979 *Phys. Rev.* C **20** 576
Ho H, Albrecht R, Dünnweber W, Graw G, Steadman SG, Wurn JP, Disdier D, Rauch V and Scheibling F 1977 *Z. Phys.* A **283** 234
Hoffmann H, Gregoire C, Lucas R and Ngô C 1979 *Z. Phys.* A **293** 229–40
Huizenga JR, Birkelund JR, Schröder WU, Wolf KL and Viola VE 1976 *Phys. Rev. Lett.* **37** 885
Ishihara M, Numao J, Fukada T, Tanaka K and Inamura T 1976 *Proc. Symp. on Macroscopic Features of Heavy-Ion Collisions, Argonne, Illinois* ed DG Kovar *ANL Rep. No* ANL-PHY-76-2, p 617
Jacmart JC, Colombani P, Doubre H, Frascaria N, Poffé N, Riou M, Roynette JC and Stephan C 1975 *Nucl. Phys.* A **242** 175
Kaufmann R and Wolfgang R 1959 *Phys. Rev. Lett.* **3** 232
Kratz JV, Ahrens H, Bogl W, Bruchle W, Franz G, Schadel M, Warnecke I, Wirth G, Klein G and Weis M 1977 *Phys. Rev. Lett.* **39** 948–87
Kratz JV, Norris AE and Seaborg GT 1974 *Phys. Rev. Lett.* **33** 502
Lauterbach C, Dünnweber W, Graw G, Hering W, Puchta H and Trautmann W 1978 *Phys. Rev. Lett.* **41** 1774–7

Lebrun C, Hanappe F, Lecolley J F, Lefebures F, Ngô C, Peter J and Tamain B 1979 *Nucl. Phys.* A **321** 207–12
Lefort M and Ngô C 1978 *Ann. Phys., NY* **3** 5
Mathews G J and Moretto L G 1979 *Phys. Lett.* **87B** 331–4
Mathews G J, Wozniak G J, Schmitt R P and Moretto L G 1977 *Z. Phys.* A **283** 247
Miller J A, Catchen G L, Logan D, Rajagopalan M, Alexander J M, Kaplan M and Zisman M S 1978 *Phys. Rev. Lett.* **40** 100
Moretto L G 1975 *Nucl. Phys.* A **247** 211
—— 1978 *J. Phys. Soc. Japan* **44** *Suppl.* 7 369
—— 1979 *Proc. Varenna Conf., Varenna, Italy July 9–25* (to be published) *Lawrence Berkeley Lab. Rep. No* LBL–9130
Moretto L G, Albiston C R and Mantzouranis G 1980 *Phys. Rev. Lett.* **44** 924
Moretto L G, Galin J, Babinet R, Fraenkel Z, Schmitt R, Jared R and Thompson S G 1976 *Nucl. Phys.* A **259** 172
Moretto L G, Heuneman D, Jared R C, Gatti R C and Thompson S G 1973 *Physics and Chemistry of Fission* vol 2 (Vienna: IAEA) p 351
Moretto L G and Schmitt R P 1976 *J. Physique* **37** C5 109
—— 1980 *Phys. Rev.* C **21** 204
Moretto L G and Sventek J S 1975 *Phys. Lett.* **58B** 26
Moretto L G, Sventek J S and Mantzouranis G 1979 *Phys. Rev. Lett.* **42** 563
Natowitz J B, Namboodiri M N, Kasiraj P, Eggers R, Adler L, Gonthier P, Cerruti C and Alleman T 1978 *Phys. Rev. Lett.* **40** 751–4
Nix J R 1969 *Nucl. Phys.* A **130** 241
Nix J R and Sierk A J 1977 *Phys. Rev.* C **15** 2072–82
Nix J R and Swiatecki W J 1965 *Nucl. Phys.* **71** 1
Nomura T, Utsunomiya H, Motobayashi T, Inamura T and Yanokura M 1978 *Phys. Rev. Lett.* **40** 694
Nörenberg W 1974 *Phys. Lett.* **52B** 289
—— 1975 *Z. Phys.* A **274** 241
—— 1976 *J. Physique* **37** C5 141
Nörenberg W and Riedel C 1979 *Z. Phys.* A **290** 335–6
Nörenberg W and Weidenmuller H A 1980 *Lecture Notes in Physics* **51**
Oeschler H, Wagner P, Coffin J P, Engelstein P and Heusch B 1979 *Phys. Lett.* **87B** 193–7
Olmi A, Sann H, Pelte D, Eyal Y, Gobbi A, Kohl W, Lynen U, Rudolf G, Stelzer H and Bock R 1978 *Phys. Rev. Lett.* **41** 668–91
Otto R J, Fowler M, Lee D and Seaborg G T 1976 *Phys. Rev. Lett.* **36** 135
Plasil F, Burnett D S, Britt H C and Thompson S G 1966 *Phys. Rev.* **142** 696
Puigh R J, Doubre H, Lazzarini A, Steamster A, Vandenbosch R, Zisman M S and Thomas T D 1980 *Nucl. Phys.* A **336** 279–89
Randrup J 1978 *Nucl. Phys.* A **307** 319–48
—— 1979 *Nucl. Phys.* A **327** 490–516
Regimbart R, Behkami A, Wozniak G J, Schmitt R P, Sventek J S and Moretto L G 1978 *Phys. Rev. Lett.* **41** 1355
Rivet M F, Bimbot R, Fleury A, Gardes D and Llabador Y 1977 *Nucl. Phys.* A **276** 157
Robel M 1979 *PhD Thesis. Lawrence Berkeley Lab. Rep. No* LBL-8181
Russo P, Schmitt R P, Wozniak G J, Jared R C, Glässel P, Cauvin B, Sventek J S and Moretto L G 1977 *Nucl. Phys.* A **281** 509
Schmitt R P, Bizard G, Wozniak G J and Moretto L G 1978 *Phys. Rev. Lett.* **41** 1152
Schröder W U, Birkelund J R, Huizenga J R, Welke W W and Randrup J 1980 *Phys. Rev. Lett.* **44** 300–12
Schröder W U, Birkelund J R, Huizenga J R, Wolf K L and Viola V E Jr 1978 *Phys. Rep.* **45** 301–43
Schröder W U and Huizenga J R 1977 *Ann. Rev. Nucl. Sci.* **27** 465
Simbel M H and Adul-Magd A Y 1980 *Z. Phys.* A **294** 277
Siwek-Wilczynska K and Wilczynski J 1976 *Nucl. Phys.* A **264** 115
Specht H J 1979 *Lecture Notes in Physics* **92** 1
Sventek J S and Moretto L G 1978 *Phys. Rev. Lett.* **49** 697
Swiatecki W J 1979 *Int. School of Nuclear Physics 'Ettore Majorana' Center for Scientific Culture, Erice-Trapani, Sicily, March* 26–*April* 6 (to be published) *Lawrence Berkeley Lab. Rep. No* LBL–8950
Tamain B *et al* 1979 *Nucl. Phys.* A **330** 253
Trautmann W, de Boer J, Dünnweber W, Graw G, Kopp R, Lauterbach C, Puchta H and Lynen U 1977 *Phys. Rev. Lett.* **39** 1062–5

Tsang CF 1974 *Phys. Scr.* **10A** 90
Van Bibber K, Ledoux R, Steadman SG, Videbaek F, Young G and Flaum C 1977 *Phys. Rev. Lett.* **38** 334–7
Vandenbosch R 1979 *Phys. Rev.* C **20** 171–5
Volkov VV 1978 *Phys. Rep.* **44** 93–157
Weiner R and Weström M 1975 *Phys. Rev. Lett.* **34** 1523
Wilczynski J 1973 *Phys. Lett.* **47B** 484–86
Wilhelmy JB, Cheifetz E, Jared RC, Thompson SG, Bowman HR and Rasmussen JO 1972 *Phys. Rev.* C **5** 2041–60
Wirth G, Bruchle W, Gaggeler H, Kratz JV, Schadel J, Warneke I, Herrmann G, Weis M, Lucas R and Poitou J 1979 *Proc. Int. Workshop on Gross Properties of Nuclei and Nuclear Excitations VII, Hirschegg, Austria* INKA-Conf-79-001-001/INKA-Conf-79-001-039 13
Wolf KL, Unik JP, Huizenga JR, Birkelund JR, Freiesleben H and Viola VE 1974 *Phys. Rev. Lett.* **33** 1105
Wolschin G 1979 *Phys. Lett.* **88B** 35–8
Wolschin G and Nörenberg W 1978a *Z. Phys.* A **284** 209–16
—— 1978b *Phys. Rev. Lett.* **41** 691–4
Wozniak GJ, Schmitt RP, Glässel P, Jared RC, Bizard G and Moretto LG 1978 *Phys. Rev. Lett.* **40** 1436
Wozniak GJ *et al* 1980 *Phys. Rev. Lett.* **45** 1081–4
Zielinska-Pfabe 1978 *M. Nucleonika* **23** 113–7

This report was done with support from the Department of Energy. Any conclusions or opinions expressed in this report represent solely those of the author(s) and not necessarily those of The Regents of the University of California, the Lawrence Berkeley Laboratory or the Department of Energy.

Reference to a company or product name does not imply approval or recommendation of the product by the University of California or the U.S. Department of Energy to the exclusion of others that may be suitable.

TECHNICAL INFORMATION DEPARTMENT
LAWRENCE BERKELEY LABORATORY
UNIVERSITY OF CALIFORNIA
BERKELEY, CALIFORNIA 94720